BB

GSI

GSI-Preprint-97-29
Mai 1997

DECAY PROPERTIES OF VERY NEUTRON-DEFICENT ISOTOPES OF SILVER AND CADMIUM

K. Schmidt, P.C. Divari, Th.W. Elze, R. Grzywacz, Z. Janas, I.P. Johnstone, M. Karny, H. Keller, R. Kirchner, O. Klepper, A. Plochocki, E. Roeckl. K. Rykaczewski, L.D. Skouras, J. Szerypo, J. Zylicz

(Accepted for publication in Nucl. Phys. A)

Gesellschaft für Schwerionenforschung mbH
Planckstraße 1 • D-64291 Darmstadt • Germany
Postfach 11 05 52 • D-64220 Darmstadt • Germany

Decay properties of very neutron-deficient isotopes of silver and cadmium

K. Schmidt [a,1], P.C. Divari [b], Th.W. Elze [c], R. Grzywacz [d], Z. Janas [d], I.P. Johnstone [e], M. Karny [d], H. Keller [a,1], R. Kirchner [a], O. Klepper [a], A. Płochocki [d], E. Roeckl [a], K. Rykaczewski [d,2], L.D. Skouras [b], J. Szerypo [d], and J. Żylicz [d]

[a] *GSI, Darmstadt, D-64291 Darmstadt, Germany*

[b] *Institute of Nuclear Physics, N.C.S.R. Demokritos, GR-15310 Aghia Paraskevi, Greece*

[c] *Institut für Kernphysik, Universität Frankfurt/Main, D-60486 Frankfurt/Main, Germany*

[d] *Institute of Experimental Physics, University of Warsaw, PL-00681 Warsaw, Poland*

[e] *Department of Physics, Queens University, Kingston, Ontario. Canada K7L 3N6*

The β-decay properties of the lightest known silver and cadmium isotopes are investigated. Data for β-delayed γ-ray emission of $^{95-97}$Ag and for β-delayed proton emission of ^{96}Ag and ^{97}Cd are presented. The experimental findings are compared with predictions of shell-model calculations in which a variety of model spaces and effective interactions are considered.

Keywords: RADIOACTIVITY ^{95}Ag [from ^{58}Ni(^{40}Ca,p2n), E=4.0-4.5 MeV/u], ^{96}Ag [from ^{60}Ni(^{40}Ca,p3n), E=4.1 MeV/u], ^{97}Ag [from ^{60}Ni(^{40}Ca,p2n), E=4.1 MeV/u], ^{97}Cd [from ^{60}Ni(^{40}Ca,3n), E=4.2 MeV/u]; measured E_γ, I_γ, $\gamma\gamma$ coin, Xγ coin, E_p, I_p, $p\gamma$ coin, $T_{1/2}$; deduced *log ft*, J, π. On-line mass separation, Ge-detectors, Si(Li) detectors. NUCLEAR STRUCTURE ^{95,96,97}Pd, ^{97}Ag; calculated levels, Gamow-Teller strength. SHELL MODEL

---

[1] Present address: SAP AG, PO Box 1461, D-69185 Walldorf, Germany

[2] Present address: Oak Ridge National Laboratory, Physics Division, PO Box 2008, Oak Ridge, Tennessee 37831-6371, USA

1 Introduction

The area around the doubly-magic nucleus ^{100}Sn [1,2] is a unique testing ground for nuclear structure physics in many respects. Examples of the various phenomena which have attracted experimental as well as theoretical interest, are mass measurements [3], mapping of the proton drip line, direct charged-particle radioactivity [4] maybe even including cluster emission [5] and β-decay with unusually large energy release [6]. Due to the closed core at $N = Z = 50$, detailed comparisons between experimental results and shell-model calculations become feasible. Moreover, nuclear structure data in this part of the chart of nuclei provide valuable input data for calculations in the framework of the astrophysical rp-process ([7] and references therein).

In this paper we present recent investigations of β-decay properties of the lightest known silver and cadmium isotopes. While a previous publication [8] dealt with the β-delayed proton (βp) emission from ^{94}Ag and ^{95}Ag, this report contains results for the β-delayed γ-ray ($\beta\gamma$) emission from ^{95}Ag, ^{96}Ag and ^{97}Ag. Furthermore, βp data for ^{96}Ag and ^{97}Cd are discussed. The aim of these measurements is to use $\beta\gamma$ and βp data for a determination of the β-intensity as a function of excitation energy in the daughter nucleus, including eventually an experimental limit for the observation of the β-intensity, in particular at high excitation energy. Finally, the experimental findings are compared to shell-model predictions.

Nuclear β-decay in the region of interest to this paper follows an easy pattern. Protons predominantely occupy the $g_{9/2}$ shell. Therefore, two channels for allowed β^+-decay are available: i. e. $\pi g_{9/2} \rightarrow \nu g_{9/2}$ and $\pi g_{9/2} \rightarrow \nu g_{7/2}$. Since $N = 50$ is expected to be a good core for neutrons, the transitions to the $\nu g_{9/2}$-orbit generally dominate the experimental spectrum for final states with $N \leq 50$ neutrons. On the other hand, the transition $\pi g_{9/2} \rightarrow \nu g_{7/2}$ is mainly responsible for the decay to nuclei with $N > 50$ neutrons. In either case the effects of the less-favoured transition, as well of others like those involving a $\pi g_{7/2}$ orbit, are normally taken into account by a renormalization of the Gamow-Teller (GT) operator [9–11]. The renormalization of the operator has been shown [9–11] to account for part of the observed quenching of the GT strength (see e. g. [12,13] for recent reviews).

Another feature of very neutron-deficient nuclei is the decay mode of βp emission. Prerequisites of this kind of disintegration are (i) a large energy window, defined by the difference of the β-decay energy (Q_{EC}) and the proton separation energy in the daughter nucleus (S_p), and (ii) substantial β-feeding of highly excited states in the daughter nucleus. On the basis of the (Q_{EC}-S_p) values, listed in Table 1, one expects sizeable branching ratios for βp emission ($b_{\beta p}$) in the case of ^{95}Ag, ^{96}Ag and ^{97}Cd.

Finally, a further interesting characteristic of isotopes in the ^{100}Sn region is the occurrence of isomers. These states mainly appear due to two reasons. The first is hole excitations from the $p_{1/2}$ shell which result in the production

of low-spin isomers in odd-A nuclei. The second reason is that the residual interaction between a proton and a neutron in the $g_{9/2}$ shell produces states with large spin differences, like the 0^+ and 9^+, which are very close in energy. This behaviour results in high-spin isomers in odd-A nuclei, like the $23/2^+$ level in ^{95}Ag and the $25/2^+$ state in ^{97}Cd [16], the properties of which are investigated in this work. Apart from electromagnetic transitions, β-decay is a possible deexcitation mode for both kinds of isomers. Therefore, it can be expected that the experimental $\beta\gamma$ or βp data for odd-A and odd-odd nuclei will comprise a mixture of different decay modes.
In this context, it should be mentioned, that the investigation of β-decay properties is only one way to extract nuclear structure information. In-beam spectroscopy constitutes another established method to achieve this goal (see e.g. [17] for a status report). The results of these two techniques often render complementary results.
This paper is structured as follows: The experimental set-up is described in sect. 2 and the measured data are presented in sect. 3. The shell-model calculations are described in sect. 4 while sect. 5 contains a comparison between experimental findings and shell-model predictions. Finally, sect. 6 gives the summary and the outlook.

2 Experimental techniques

The neutron-deficient isotopes of silver and cadmium were produced by fusion-evaporation reactions of a ^{40}Ca beam from the heavy-ion accelerator UNILAC with targets of ^{58}Ni or ^{60}Ni. By using a niobium degrader, the beam energy was reduced to the values given in Table 2. The intensity of the incident beam amounted to approximately 50 particle nA. The reaction products were separated at the GSI On-line Mass Separator by using a chemically selective FEBIAD-B2 ion source with an uncooled tantalum coldpocket [18]. This set-up provided clean secondary beams of silver, while strongly suppressing possible palladium and rhodium isobars. Furthermore, the release from the ion source was fast enough to avoid serious losses in intensity for isotopes with half-lives down to 50 ms [19]. The mass-separated ion beams were implanted into a tape and accumulated for a specific time, i.e. the cycle time given in Table 2. The resulting radioactive sources were moved periodically to measuring positions equipped with two different experimental set-ups. The first array of detectors (labelled as $\Delta E - E$ in Table 2) consisted of a $\Delta E - E$ telescope for βp detection and two large-volume germanium detectors for $\gamma-$ and X-ray spectroscopy. Another set-up (marked as $\gamma - \gamma - X$ in Table 2) was constructed using three germanium detectors for recording $\gamma - \gamma - X$ coincidences. The telescope was made up by two silicon detectors with thicknesses of 26 μm and 725 μm and active areas of 150 mm^2 and 450 mm^2, respectively. By applying

a coincidence condition between these detectors, βp energy and time spectra were recorded. The energy resolution of the sum-energy spectrum was of the order of 40 keV FWHM for a proton energy of 3 MeV.
The data acquisition was synchronized to the cycle time. The events of the $\Delta E - E$ telescope and the germanium detectors were stored as listmode data. In addition, time-sequential multispectrum data were taken from the $\gamma-$ and X-ray counters. Standard $\gamma-$ray sources were used to determine the absolute efficiency of the $\gamma-$ and X-ray detectors, and to deduce the $\gamma-$energy calibration. The latter procedure, which also took known $\gamma-$lines from room background and isobaric contaminants into account, yielded the energies of $\gamma-$transitions in ^{95,96,97}Pd with uncertainties of ± 0.5, ± 1, and ± 2 keV for the $\gamma-$energy intervals of 0-1, 1-2, and 2-3.3 MeV, respectively. The experimental $\gamma-$ray intensities were corrected [20] for summing effects occuring with respect to coincident $\gamma-$ray cascades, 511 keV quanta and/or positrons. The largest dead time of the data acquisition system for the multispectrum mode, which occured for the ^{97}Ag measurement, amounted to a value of only 0.33% averaged over the 40 s cycle time. Therefore, dead time corrections were neglected in the determination of half-lives.
The parameters that are relevant for the production of the nuclei of interest and for the detection of their decay radiation are summarized in Table 2. In addition to details discussed so far, the total measuring time for each isotope is listed. Fig. 1 shows as an example the γ-ray singles spectrum obtained for the ^{95}Ag decay, this case representing the weakest γ-ray activity investigated in this work.

3 Experimental results

3.1 The decay of ^{95}Ag

Experimental investigations of the β-decay of ^{95}Ag encounter a complicated situation. The ground-state properties of this isotope are expected to be essentially determined by an unpaired proton in the $\pi g_{9/2}$ shell, with allowed GT decays feeding the $11/2^+$, $9/2^+$ and $7/2^+$ states in the daughter nucleus ^{95}Pd. This decay strongly populates the ground state of ^{95}Pd, which is mainly formed by coupling a $g_{9/2}$ neutron hole to the 0^+ ground-state of ^{96}Pd. Shell-model calculations performed by Ogawa [16] show the existence of two isomers in ^{95}Ag, i. e. a $1/2^-$ level at 660 keV and a $23/2^+$ state at 2.6 MeV. The β-decay of these two states is predicted [16] to have lifetimes comparable to those of their γ-decay and should thus be observable.
Both $\beta\gamma$ and βp measurements were carried out at mass A=95. In view of the expected dominant population of the ground state of ^{95}Pd and the low intensity of the ^{95}Ag samples, the search for β-delayed γ-rays of ^{95}Ag is not

an easy task. Energies, intensities, half-lives and $\gamma\gamma$ coincidence relations for the $\beta\gamma$ transitions attributed to the decay of ^{95}Ag are compiled in Table 3. The weighted mean of the half-life, determined from the γ-ray data listed in this table, amounts to $T_{1/2}(^{95}Ag, \beta\gamma) = (1.74 \pm 0.13)$ s. The βp activity observed at A=95 has a half-life of $T_{1/2}(^{95}Ag, \beta p) = (2.0 \pm 0.1)$ s [8]. The somewhat longer half-life measured for the βp emission probably originates in a small admixture of the 13.3 s activity of the β-decay daughter ^{95}Pd [21]. (As mentioned in sect. 2, the release of palladium isotopes from the ion source is suppressed). Therefore, we consider the $\beta\gamma$ and βp data to represent one and the same activity characterized by a half-life of (1.74 ± 0.13) s, and assign them, in accordance with our previous work [8], and with the shell-model results described in sect. 5.1, to the decay of the $9/2^+$ ground-state of ^{95}Ag.
The experimental data on the β-decay of ^{95}Pd were restricted so far to the disintegration of the $21/2^+$ isomer [21,22]. In addition to confirming several of the β-delayed γ-rays measured in these works, we were able to deduce limits for the half-life $T_{1/2}(^{95g}Pd, \beta\gamma)$ of the ^{95}Pd ground-state. From an analysis of the time characteristics of Rh K_α X-rays and of the 1350.9 keV transition in ^{95}Rh, we found $1.7s \leq T_{1/2}(^{95g}Pd, \beta\gamma) \leq 7.5s$ [20]. A γ-ray line of 1219.3 keV (see fig. 1) was observed to have a half-life of (1.35 ± 0.26) s and a coincidence relation with the 1350.9 keV transition in ^{95}Rh. The assignment of this line remains unclear. The experimental decay scheme of ^{95}Ag as derived from the $\beta\gamma$ data is illustrated in fig. 2. Although the time characteristic of the 1799.8 keV transition is compatible with a half-life of 1.74 s, the low intensity did not allow for the determination of the half-life or the measurement of $\gamma\gamma$ coincidences. Therefore, energy-sum considerations were used to place this γ-line in the level scheme. Due to the low source strength of the ^{95}Ag samples (see fig. 1) and the correspondingly scarce coincidence data, the decay scheme displayed in fig. 2 represents only a first approximation and does, e. g., not contain β-intensities or a $b_{\beta p}$ value. A determination of the GT strength from these data has not been attempted.
Additional γ-ray activites with time characteristics different from those described in this work, or known from previous experiments, were not perceived for A=95. The β-decay of the predicted $23/2^+$ isomer in ^{95}Ag (see sect. 5.1), for example, would populate the $23/2^+$ state in ^{95}Pd, which is known [23] to be de-excited by a 691 keV γ-transition. However, the poor quality of our $\beta\gamma$ data does not allow us to use the non-observation of this γ-line for a quantitative estimate of the half-life or the limit of the production rate of this isomer. Thus, we are unable to deduce evidence from our data for the β-decay of the isomeric $1/2^-$ or $23/2^+$ states (see sect. 5.1) in ^{95}Ag.

3.2 The decay of ^{96}Ag

The calculations presented in sect. 5.2 predict two nearly degenerate levels with spins of 8^+ and 2^+ as candidates for the ground state of ^{96}Ag. Therefore, no direct feeding of the 0^+ ground-state of ^{96}Pd by allowed β-decays is expected. In a previous experiment on ^{96}Ag, Kurcewicz et al. [22] investigated βp and $\beta\gamma$ emission, measured the half-life to be $(5.1 \pm 0.4)s$, and determined a $b_{\beta p}$ value of (8.0 ± 2.3) % (Note that a large $b_{\beta p}$ value is expected for ^{96}Ag due to the wide $(Q_{EC} - S_p)$ window stemming from the $N = 50$ shell closure at ^{96}Pd, see Table 1). Moreover, data from in-beam experiments on ^{96}Pd [24,25] are available.

The decay studies described in this chapter slightly modify the results obtained by Kurcewicz *et al.* [22]. The βp spectrum shown in fig. 3, is characterized by a striking fine-structure. This observation can be qualitatively interpreted as being due to the Z=50, N=50 shell closure and the correspondingly low density of excited levels in ^{96}Pd (N=50). However, a fluctuation analysis (see [26] for a recent review) of this spectrum seems to be excluded in view of the limits of our data with respect to counting statistics and energy resolution. The half-life inferred from the βp data amounts to $T_{1/2}(^{96}Ag, \beta p) = (5.22 \pm 0.15)$ s (see fig. 3). Table 4 depicts the results for the γ-lines attributed to the disintegration of ^{96}Ag. The weighted mean of the half-lives of all $\beta\gamma$ transitions is $T_{1/2}(^{96}Ag, \beta\gamma) = (4.50 \pm 0.06)$ s. The observation of two different half-life values for ^{96}Ag is interpreted as being due to the existence of the 2^+ and 8^+ decays, as will be discussed in more detail in sect. 5. Fig. 4 shows the decay scheme deduced from the $\beta\gamma$ data. The intensities were normalized to the number of β-decays observed, which was determined as the sum of the experimental βp intensity and the events measured for the 1415.5 keV γ-transition, taking the respective detection efficiencies into account. In accordance with the data from previous β-decay and in-beam experiments [22,24,25] and with the shell-model results presented in sect. 5, the γ-transitions are interpreted as an $8^+ \rightarrow 6^+ \rightarrow 4^+ \rightarrow 2^+ \rightarrow 0^+$ yrast cascade. The intensity of the 106.6 and 325.3 keV transitions were corrected for internal conversion.The *log ft* values were calculated using the half-life of $T_{1/2}(^{96}Ag, \beta\gamma) = (4.50 \pm 0.06)$ s, the intensities given in fig. 4, and the f-values from ref. [27]. Moreover, the $b_{\beta p}$ value was determined by comparing the proton intensity to that of the 1415.5 keV transition. The new value of $b(\beta p) = (11.9 \pm 2.6)$ % is in good agreement with the result obtained by Kurcewicz *et al* [22].

3.3 β-delayed γ-ray emission from ^{97}Ag

The ground state of ^{97}Ag consists of an unpaired proton in the $\pi g_{9/2}$ shell. Therefore, the same decay channels as in the case of ^{95}Ag are available. In

contrast to the ^{95}Ag decay, however, the ground state of the daughter nucleus ^{97}Pd is, due to its $\nu d_{5/2}$ configuration, not populated via allowed β-decay. Thus, the determination of the *log ft* values, which depend on the absolute $\beta\gamma$ intensities, becomes feasible with the experimental set-up described in sect. 2. In complete analogy to the case of ^{95}Ag, the presence of a low-lying $1/2^-$ isomer is expected. Previous experimental investigations of the β-decay of ^{97}Ag [28,22] rendered a rather incomplete picture with only two $\beta\gamma$ transitions and values of (21 ± 3) s [28] and (17 ± 3) s [22] for the half-life of this isotope. In-beam experiments on ^{97}Pd [29,30] have yielded detailed information on excited levels and spins, while Alber *et al.* [31] were able to prove the existence of an $21/2^+$ isomer at an excitation energy of 2.343 MeV in ^{97}Ag.
The experimental $\beta\gamma$ data for ^{97}Ag are given in Table 5. The half-life was determined from the strongest γ-ray transitions; the weighted mean of the values listed in Table 5 amounting to (25.3 ± 0.3) s. The discrepancy between this value and the results obtained by Huyse *et al.* [28] and Kurcewicz *et al.* [22], respectively, is not understood. The coincidence relations allowed for the construction of the decay scheme depicted in fig. 5. The spins and the parities of the ^{97}Pd levels shown in this figure can partly be taken from in-beam work [29,30], while the *log ft* values were calculated by using the half-life of 25.3 s and a Q_{EC} value of 7.0 MeV (see Table 1). In addition to the γ-data listed in Table 5, another γ-ray with an energy of $E_\gamma = 1043.0$ keV and a half-life of $T_{1/2} = (17.2 \pm 2.1)$ s was registered. Since no coincidences could be determined for this transition, its actual origin remains unclear. The predictions of shell-model calculations about the possibility of an isomeric decay are discussed in sect. 5.3

3.4 The decay of ^{97}Cd

The decay of the lightest known cadmium isotope, ^{97}Cd, is governed, similarly to the decay of ^{96}Ag, by the closed neutron shell ($N = 50$) in the daughter nucleus ^{97}Ag. Correspondingly, a large $(Q_{EC} - S_p)$ window (see Table 1) and a significant $b_{\beta p}$ value are expected. Previous experimental investigations [32,22], as well as this work, have therefore focused on the βp decay mode. The only nuclear properties measured for ^{97}Cd prior to our experiment were the occurrence of βp emission [32] and the half-life of (3^{+4}_{-2}) s [22]. A particularly interesting feature of this isotope is the predicted existence [16] of the $25/2^+$ isomer at an excitation energy of 2.4 MeV. The decay properties of such a state are discussed in sect. 5.4.
The results of our βp measurement are depicted in fig. 6. This is the first time, that a βp energy spectrum has been obtained for this exotic nucleus. The new half-life value for ^{97}Cd from this work is (2.8 ± 0.6) s. Furthermore, the analysis of the proton-γ coincidence data yielded traces of a coincidence relation between the β-delayed protons and the 325.3 keV as well as the 684.0

keV transitions in ^{96}Pd. Since these two γ-rays form a $6^+ \rightarrow 4^+ \rightarrow 2^+$ cascade, it can be assumed that the observed βp activity stems from the ground-state decay of ^{97}Cd, whose spin/parity assignment is presumably $9/2^+$. However, due to the low statistics of the proton-γ coincidence data, an admixture of other activities, such as the $25/2^+$ isomer, cannot be excluded.

4 The shell-model calculations

Most of the nuclei examined in this paper, namely $^{95-97}$Ag, $^{95-96}$Pd and ^{97}Cd, have $N \leq 50$ and therefore are described in terms of neutron holes with respect to the $N = 50$ core. However, the study of the β^+ decay of ^{97}Ag requires the determination of the wavefunctions of the daughter nucleus ^{97}Pd which has $N = 51$ neutrons. To study these two groups, i.e the $N \leq 50$ and the $N > 50$ nuclei, it was necessary to perform two different types of calculation. These are described in the following sections 4.1 and 4.2 while the results of the calculations are compared with experimental findings in sect. 5.
For nuclei closer to the β-stability line, the aim of a calculation is normally to interpret the rather complete set of experimental data. In the case of exotic nuclei, however, where experimental data are scarce, the basic aim of a calculation is to make predictions about the properties of these nuclei, which may be useful to experimentalists in planning their measurements or analysing their (scarce) data. For these predictions to be reliable, one has to employ a model which has been tested to describe satisfactorily the observed properties of neighbouring nuclei. Of course, there is no guarantee that a model will be succesful outside the region in which it has been tested. A safer approach, therefore, is to determine the properties of the exotic nuclei using different models and to compare their predictions. This policy has been adopted in the present work. Thus for each of the two groups of nuclei, i.e the $N \leq 50$ and $N > 50$, we have made two independent studies using models which differ not only in the definition of the model space but also in the manner in which the effective interaction is determined.

4.1 The $N \leq 50$ nuclei

A shell-model study of nuclei with proton number $37 \leq Z \leq 46$ and neutron number $48 \leq N \leq 50$ was recently reported by Sinatkas *et al.* [33,34]. In this calculation the doubly-closed ($Z = N = 50$) ^{100}Sn is assumed as inert core and the nuclei under consideration are described in terms of proton and neutron holes which are distributed in the $g_{9/2}$, $p_{1/2}$, $p_{3/2}$ and $f_{5/2}$ orbitals. The effective operators appropriate for this model, like the two-body interaction and the one-body electromagnetic operators, have been determined by con-

sidering second order corrections to the corresponding bare operators. Thus, the calculation of Sinatkas *et al.* contains only six free parameters, three one-hole energies and three parameters modifying the strength of certain proton-neutron matrix elements, the values of which have been determined [33,34] by a least-square fit to the experimental level energies of $N = 50, 49$ nuclei.

A different approach was adopted by Gloeckner and Serduke [35], Serduke, Lawson and Gloeckner [36], and Gross and Frenkel [37] (see Grawe et al. [17] for a recent review) for the study of nuclei with $Z > 38$ and $N \leq 50$. In these calculations, ^{88}Sr is considered as core and the nuclei under consideration are described in terms of proton-particles and neutron-holes distributed in the $g_{9/2}$ and $p_{1/2}$ orbitals. The matrix elements of the effective hamiltonian have been determined [35–37] by a least-square fit to the observed level energies of $Z > 38$ and $N \leq 50$ nuclei.

In the present study we employ both the above described models to determine the properties of $^{95-97}$Ag, $^{95-96}$Pd and ^{97}Cd nuclei. To avoid confusion we shall describe in the following as Model-1 and Model-2 the calculations in the large and small spaces, respectively. The new experimental data, obtained in this work, present a suitable broad basis to test the predictions of these two models. Our results are also compared to those obtained by Ogawa [16], who made the first shell-model study of the neutron-deficient isotopes with $N \leq 50$. Ogawa's calculations were performed in the same model space as in the Model-2 approach but differ from ours in the choice of the effective interaction. Thus in our Model-2 calculations we use the SLG interaction [35,36] while Ogawa [16] employed the interaction derived by Gross and Frenkel [37]. In our calculations of the β^+-decay of the $N \leq 50$ nuclei we employ a renormalized GT operator. This was determined by adding to the bare operator the effects of core polarization. A diagrammatic representation of this correction is shown in fig. 7.

Quite recently an extension of Model-2 was introduced by Johnstone and Skouras [38]. In this new model, to be referred to as Model-2e, the restriction of a rigid $N = 50$ core is relaxed and single-particle excitations are allowed to occur from the $p_{1/2}$ and $g_{9/2}$ orbits into the $g_{7/2}$, $d_{5/2}$, $d_{3/2}$ and $s_{1/2}$ shells. The effective interaction for this model space was determined [38] by least-squares fits to known levels of $N = 50, 49$ nuclei.

Calculations employing Model-2e have the following two advantages over those using Model-1 or Model-2: i) since the $\pi g_{7/2}$ orbit is directly included in the model space, there is no need to renormalize the GT operator (see fig. 7), and ii) since particle-hole excitations can carry up to 8 units of angular momentum, one can describe with Model-2e high-spin states which cannot be described in the model space employed by the other two models. Indeed Johnstone and Skouras [38] using Model-2e were able to give a very satisfactory description of the observed high-spin states of $N = 50$ nuclei. On the other hand, the results of the calculation in ref. [38] show that for the low-lying states of the $N = 50$ nuclei the effects of particle-hole excitations are small and can be satisfactorily taken into account with the use of effective operators. For this

reason, but also in order to avoid extensive computations, the use of Model-2e in this work is restricted only to the study of the GT decay of the $25/2^+$ state of ^{97}Cd (see sect. 5.4).

4.2 The decay of ^{97}Ag

The β-decay of the $N = 50$ nuclei has been the subject of several shell-model studies [9–11,40]. In the present calculation of the decay of ^{97}Ag we closely follow the procedure introduced in two of these earlier investigations [10,11]. Below we give a brief description of these two approaches.
In the first approach, hereafter called Model-3, the doubly closed nucleus ^{100}Sn is considered as inert core. The valence space consists of the $g_{9/2}$, $p_{1/2}$, $p_{3/2}$ and $f_{5/2}$ proton-hole orbitals and the $g_{7/2}$, $d_{5/2}$, $d_{3/2}$ and $s_{1/2}$ neutron-particle ones. The effective two-body interaction has been determined by considering second-order corrections to the G-matrix while single-particle energies have been determined by a least-square fit to the observed levels of $N = 51$ nuclei [41]. Effective one-body and two-body GT matrix elements, appropriate for the model space of the calculation, have been determined in a manner similar to that described in ref. [11].
A different approach has been followed by Johnstone [10] in his investigation of the GT decay of the $N = 50$ nuclei. In this case, ^{88}Sr is assumed as inert core and the valence protons are placed in the $g_{9/2}$ and $p_{1/2}$ orbitals, while the single valence neutron of the $N = 51$ nuclei, like in the Model-3 case, is allowed to occupy any of the $g_{7/2}$, $d_{5/2}$, $d_{3/2}$ and $s_{1/2}$ orbitals. The matrix elements of the effective hamiltonian for this model space have been determined by a fitting procedure to the observed spectra of the $N = 51$ nuclei [10]. Finally, the β^+-decay of the $N = 50$ nuclei has been determined by Johnstone [10] by considering a renormalized GT operator which contains both one-body and two-body corrections. This calculation will be referred to in the following as Model-4.
It should be noticed that Model-3, when applied to $N = 50$ nuclei, produces results identical to those obtained from a Model-1 calculation and a similar situation occurs between Model-2 and Model-4. This has been accomplished by using in Model-3 [11] and Model-4 [10] the same proton effective hamiltonian as in the Model-1 and Model-2 calculations, respectively.

5 Comparison between experimental results and shell-model predictions

In the following sections 5.1 to 5.4 we present the theoretical predictions of energy spectra and decay properties of the neutron-deficient isotopes $^{95-97}$Ag

and ^{97}Cd and compare them to the experimental data.
In order to determine GT lifetimes, we have calculated the Q_{EC} values shown in Table 1. In the case of $^{95-96}$Ag and ^{97}Cd decays, the Q_{EC} values given in Table 1 have been determined using Model-2, which has been designed [35–37] to fit the binding energies of $N \leq 50$ nuclei. On the other hand, the Q_{EC} value of ^{97}Ag has been determined using the results of a Model-4 calculation of the binding energies of $N \geq 50$ nuclei [42].
As can be seen from Table 1, there is very close agreement between the theoretical Q_{EC} values of $^{95-97}$Ag and the experimental estimates. However, in the case of ^{97}Cd, the shell-model value is more than 1 MeV higher than the typical result obtained from mass predictions [14].

5.1 The decay of ^{95}Ag

The low-energy level scheme of ^{95}Ag was first determined by Ogawa [16]. Ogawa's results are reproduced in fig. 8 where they are compared to the energy spectrum obtained using Model-1.[3] Details about both Ogawa's and Model-1 calculations may be found in sect. 4.1.
As fig. 8 shows, the energy spectra predicted by the two calculations are in very close agreement. Thus all levels predicted by Ogawa up to about 3 MeV of excitation are accounted for by our Model-1 calculation, and the excitation energies produced by the two calculations do not differ by more than 350 keV. On the other hand, there are significant differences in the predictions of the two calculations as far as the decay properties of some of the ^{95}Ag levels are concerned. The main reason for these differences arises from the fact that Ogawa's calculations were performed in a small model space, consisting of only the $p_{1/2}$ and $g_{9/2}$ orbitals, in which certain decay modes, as for example E3 decay, cannot be described.
The first instance in which E3 decay plays a significant part appears in the decay of the lowest $1/2^-$ state. This state has been predicted by Ogawa [16] to lie at 0.66 MeV and to decay by M4 transitions to the $9/2^+$ ground-state and to the first excited $7/2^+$ level, predicted to be at 36 keV. On the other hand, Model-1 predicts that the $7/2^+$ and $1/2^-$ states appear at 0.415 and 0.797 MeV excitation, respectively. The $1/2^-$ is de-excited by an E3 transition to the $7/2^+$ state. This de-excitation mode dominates, with a branching ratio of 99.7 %, over the M4 decays to the $9/2^+$ and $7/2^+$ states. The half-life corresponding to the γ-decay of the $1/2^-$ state is predicted to be 6 ms. This transition is about 200 times faster than the β^+-decay of the $1/2^-$ state, whose half-life is calculated to be 1.1 s.

[3] A preliminary presentation of the content of this section has already been given in [8]. The Model-1 results presented here are slightly different from those quoted in [8] since the present calculation was performed in a non-truncated basis.

Another case in which Ogawa's predictions differ significantly from those of Model-1 concerns the decay of the lowest $23/2^+$ state. According to Ogawa's calculation this level appears at 2.56 MeV almost degenerate with a $17/2^-$ state. It decays by M3 decay to the $17/2^+$ state at 2.08 MeV with a half-life of 0.4 s, which is comparable to its β^+ half-life of 1 s [16]. Therefore, the β^+-decay of the $23/2^+$ state should be experimentally observable.
On the other hand, our Model-1 calculation predicts the $23/2^+$ state to appear at about 2.90 MeV, i. e. well above the $17/2^-$ level at 2.31 MeV and the $17/2^+$ state at 2 34 MeV. Using these excitation energies, we find the decay of the $23/2^+$ state to have a 99.8 % branch for an E3 transition to the $17/2^-$ level. The partial half-life of the $23/2^+$ state for γ-deexcitation is predicted to be 0.4 ms, i.e. about 1000 times faster than its β^+ half-life which is found to be about 0.4 s.
The results of our Model-1 calculation indicate that it would be very difficult to observe the β^+-decay of the $1/2^-$ and $23/2^+$ isomers in ^{95}Ag. Thus, according to this calculation, the only β^+-decay observable from ^{95}Ag should originate from its ground state. The half-life of that decay is determined to be 1.26 s which is in satisfactory agreement with the experimental result of (1.74 ± 0.13) s.
As a challenge to future experiments we display in fig. 9 the B(GT) distribution predicted from our Model-1 calculation for the decay of the $9/2^+$ ground-state of ^{95}Ag. On the one hand, the dominant part of the GT strength lies above the proton separation energy of (4.51 ± 0.60) MeV in ^{95}Pd (see Table 1) so that βp measurements seem to offer a suitable probe provided the contributions from isomers in ^{95}Ag could be clarified. The latter condition cannot be fulfilled on the basis of the βp data [8] available so far. On the other hand, as far as the low-lying GT strength is concerned, the poor quality of our $\beta\gamma$ results (see figs. 1 and 2) does not allow us to deduce the distribution of the β-intensity and the related observation limit for this decay. Therefore, the comparison between experimental results and Model-1 predictions with respect to the configuration of excited ^{95}Pd levels and the B(GT) distribution for ^{95}Ag remains inconclusive. As displayed in figs. 2 and 9, Model-1 predicts that, for ^{95}Pd excitation energies between 0 and 2.3 MeV, the $9/2^+$ ground-state as well as excited levels at 1546 keV ($11/2^+$), 1662 keV ($7/2^+$) and 2069 keV ($9/2^+$) are populated. However, as can be seen from fig. 2, there is no clear correspondence between this feeding pattern and the experimental level scheme. In this context one should note that the assignment of the observed $\beta\gamma$ and βp activities to the $9/2^+$ ground-state of ^{95}Ag is only tentative so far (see sect. 3.1).

5.2 The decay of ^{96}Ag

The Model-1 calculation on ^{96}Ag shows that the ground state of this nucleus is an 8^+ state and that there is an excited 2^+ state at 19 keV. On the other hand, Model-2 predicts the 2^+ level to be the ground state and the 8^+ level to be the first excited state at 25 keV. In either case it is predicted that the first excited state of ^{96}Ag is an isomer, and that its β^+-decay, as well as that of the ground state, should be experimentally observable.
The Model-1 result for the half-life of the 8^+ state of ^{96}Ag is 5.2 s while that of Model-2 is 6.9 s. The values calculated for the half-life of the 2^+ level are 12.5 and 8.1 s, respectively. These results have to be compared with the experimental value of (4.50 ± 0.06) and (5.22 ± 0.15) s for the $\beta\gamma$ and βp activities assigned to the decay of ^{96}Ag. This comparison favours the 8^+ state as the most probable origin of both activities, even though a contribution from the 2^+ level cannot be ruled out.
The distribution of the GT strength deduced from $\beta\gamma$ data is confronted in fig. 10 with that determined from the Model-1 calculation. This figure shows that the overall agreement between the calculated and observed strength distributions is very satisfactory. According to the calculation, the largest part of the GT strength, observed at about 2.5 MeV, corresponds to the decay of the 8^+ state which predominantly feeds the first 8^+ of ^{96}Pd. On the other hand, the strength observed at about 1.4 MeV should be attributed to the decay of the 2^+ state to the first excited 2^+ level of the daughter nucleus. This observation confirms the contribution from the 2^+ decay that was already suggested on the basis of the half-life data.
The B(GT) strength for ^{96}Pd excitation energies above 5 MeV can in principle be probed by βp measurements since the proton separation energy in ^{96}Pd amounts to (5.12 ± 0.21) MeV (see Table 1). However, in view of the apparent mixture of 8^+ and 2^+ decays, we refrained from such an analysis. The ambiguity in spin/parity assignment could probably be solved by performing coincidence measurements between protons and positrons, X- and γ-rays. Such data might enable one to clarify the situation by analysing of EC/β^+ ratios and proton-feeding of ^{95}Pd states.

5.3 The decay of ^{97}Ag

Fig. 11 displays the energy spectra of ^{97}Ag obtained from the Model-1 and Model-2 calculations described in sect. 4.1. As may be seen from this figure, there is close agreement in the results of the two calculations regarding the position of the positive parity states in the spectrum. On the other hand, the agreement is less satisfactory regarding the negative parity states, which Model-2 predicts to be systematically 400-500 keV lower than Model-1.

To calculate the GT decay of ^{97}Ag, one needs first to determine the eigenstates of the daughter ^{97}Pd, which is a $N = 51$ nucleus. These have been determined employing Model-3 and Model-4, described in sect. 4.2. The half-life of the $9/2^+$ ground-state of ^{97}Ag, calculated on the basis of these eigenstates, is 19.1 and 13.8 s for Model-1 and Model-2, respectively. Both these values are in satisfactory agreement with the experimental result of (25.3 ± 0.3) s. However, the agreement of the two calculations among themselves and with experiment breaks down completely if one examines the B(GT) distribution shown in fig. 12. Thus, as seen in the figure, the results of the two calculations appear to be in reasonable agreement with each other and with experiment only up to a ^{97}Pd excitation energy of about 4.5 MeV (Note the different B(GT) scales used in fig. 12 for the data from experiment and model predictions, respectively). However, Model-1 predicts the bulk of the GT strength to lie at ^{97}Pd excitation energies of about 5 MeV, while the strength predicted by Model-2 in this region is negligible. At this point it should be remarked that due to different renormalization methods adopted in the Model-3 [11] and Model-4 [10] approaches, the total GT strength predicted by Model-3 for the decay of the ground state of ^{97}Ag is 7.12 compared to only 3.33 of Model-4. Thus, if a common renormalization method were adopted, then the agreement of the two calculations up to about 4.5 MeV would cease to exist, since then the peaks of the Model-3 distribution would be less than half of the corresponding Model-4 ones.

The discrepancy between the two calculations regarding the distribution of GT strength cannot be resolved by experiment since the experimental observation limit rises steeply above excitation energies of about 4 MeV, as can be seen from fig. 12. However, there is reasonable agreement between experiment and the two models for the low-energy part of the distribution, and this accounts for the agreement regarding lifetimes.

Among the excited states of ^{97}Ag, the case of the first $1/2^-$ level is particularly interesting. The decay properties of this state crucially depend on its excitation energy. Thus, if the $1/2^-$ state is at an excitation energy of 1.08 MeV of excitation, as predicted by Model-1, then its decay has a 83 % branch to the $7/2^+$ at 0.73 MeV, due to E3 decay, with the other 17 % corresponding to the M4 decay to the ground state. The γ-decay half-life of the $1/2^-$ state is found to be 16 ms, i.e. more than 6000 times faster than the half-life corresponding to its GT decay, which is calculated to be 101 s.

The situation changes drastically if we assume the position of the $1/2^-$ state to be 400 keV lower, as suggested by the Model-2 results. In this case the $1/2^-$ state can only be de-excited by M4 decay to the ground state of ^{97}Ag and by GT decay to the $1/2^-$ and $3/2^-$ states of ^{97}Pd. The partial half-lives predicted for the γ-transition and the β-decay from the $1/2^-$ isomer of ^{97}Ag are about 6.1 s and 380 s, respectively, which means that GT decay represents a 1.6 % branch of the total decay rate of this state.

5.4 *The decay of* ^{97}Cd

The energy spectrum of ^{97}Cd was first determined by Ogawa [16]. Ogawa's results are reproduced in fig. 13, where they are compared to the energy spectra obtained from Model-1 and Model-2 calculations. As this figure shows, there is remarkable agreement in the results of the three calculations regarding the position of the positive parity states in the spectrum of ^{97}Cd. On the other hand, there is disagreement regarding the position in the spectrum of the negative parity states. This disagreement is most remarkable in the comparison of Ogawa's and Model-2 results since, as described in sect. 4.1, these two calculations employ the same model space and effective interactions which have both been determined by a least-squares fit to the observed spectra of $N = 50, 49$ nuclei. However, ^{97}Cd is outside the range of nuclei in which the fitting procedure was applied [35–37], and the disagreement concerning negative parity states indicates the danger involved in applying a model outside the range of its validity.

The half-lives calculated for the ground-state decay of ^{97}Cd are 0.9 and 1.1 s for Model-1 and Model-2, respectively. These predictions are in satisfactory agreement with the experimental value of (2.8 ± 0.6) s, presented in sect. 3.4. As can be seen from fig. 6, good overall agreement is also obtained if the experimental βp spectrum is compared to that obtained by using the GT strength from Model-1 together with a statistical model [43]. However, this comparison does not allow us to draw any definite conclusion for two reasons. First, due to the unknown experimental $b_{\beta p}$ value an arbitrary normalization has been used for the theoretical spectrum displayed in fig. 6. Second, contributions from isomers of ^{97}Cd cannot be ruled out as will be discussed in the following.

As in the case of ^{95}Ag and ^{97}Ag, it is of particular interest to study the decay properties of the first excited $1/2^-$ state of ^{97}Cd. As can be seen from fig. 13, this state can only be de-excited by M4 decay to the ground state and by GT decay to the $1/2^-$ and $3/2^-$ states of ^{97}Ag. In the following we present the theoretical predictions regarding the decay properties of this $1/2^-$ state of ^{97}Cd. These have been obtained by using Model-1 wavefunctions, but considering the three different excitation energies of the $1/2^-$ state shown in fig. 13. Thus, if the $1/2^-$ state of ^{97}Cd appears at 1.3 MeV, as predicted by Model-1, then its total half-life is calculated to be 0.08 s with a 84 % branch for M4 decay and a 16 % branch for GT decay. If, on the other hand, the $1/2^-$ state is at 0.78 MeV, as predicted by Ogawa's calculation, then its total half-life is determined to be 0.65 s. In this case there is a dominant 93 % branch for GT decay. Finally, if the $1/2^-$ state appears at an excitation energy of only 30 keV, as predicted by Model-2, then it will decay exclusively by GT decay with a calculated half-life of 1.1 s.

As may be seen from fig. 13, all calculations predict the presence of a $25/2^+$ state at about 2.4 MeV. According to these predictions, the γ-decay of this $25/2^+$ state should be an extremely slow process, since it can only decay by

E6 decay to the $13/2^+$ state which appears about 500 keV lower. Thus the $25/2^+$ state of ^{97}Cd can only be de-excited by GT transitions to the $23/2^+$, $25/2^+$ and $27/2^+$ states of ^{97}Ag. Now, it is interesting to observe that such transitions cannot be described by either Model-1 or Model-2 since, according to these two models, ^{97}Ag can only have $21/2^+$ as highest spin.
The study of the GT decay of the $25/2^+$ state of ^{97}Cd requires a model which does not contain the restriction of a rigid $N = 50$ core. Such a model is Model-2e already described in sect. 4.1. Using this model we find that several states with spins/parities of $23/2^+$, $25/2^+$ and $27/2^+$ exist in ^{97}Ag at excitation energies between 4.8 and 13 MeV. Using their wave functions, we estimate the half-life of the $25/2^+$ state to be about 0.6 s, i.e. comparable to the half-life of the ground state of ^{97}Cd.

6 Summary and outlook

Our experiment yields the first $\beta\gamma$ data on ^{95}Ag, and constitutes, also due to the determination of the half-lives with considerably improved accuracy, the first detailed study of the β-strength distribution for the decays of ^{96}Ag and ^{97}Ag. Due to the limited quality of the experimental data and the related ambiguity concerning, e. g., the occurrence of isomerism in the parent nuclei, restrictions are imposed on the comparison between experimental and calculated GT strength distribution. In the case of ^{96}Ag and ^{97}Ag, these restrictions are evident from (i) the missing experimental sensitivity at high ^{96}Pd and ^{97}Pd excitation energies, (ii) the fact that the experimental B(GT) functions of ^{96}Ag and ^{97}Ag were exclusively based on $\beta\gamma$ data without taking βp emission into account, and (iii) the comparison between experiment and theory for ^{97}Cd was performed on the basis of βp spectra instead of B(GT) distributions.
There seem to be three possibilities for experimental improvements. One is the measurement of coincidences beween β-delayed protons and positrons, X- and γ-rays, which may help to identify contribution from isomeric decays. A second possibility is the use of the new generation of large arrays of high-resolution (germanium) detectors. This approach would definitely lower the sensitivity limit as a function of excitation energy, and would hopefully allow to quantitatively determine this limit (In this work, the latter task was only solved for the decay of ^{97}Ag, see fig. 12). A third improvement is offered by total absorption γ-ray spectrometry involving low resolution, but high-efficiency (NaI) detectors which appear to be the proper tool to study high-lying GT resonances [44].
The improvement in the experimental techniques would help to settle some of the discrepancies found in the theoretical results. Thus, knowledge of the position of the GT resonances in the decay of ^{97}Ag and of the excitation energy

and decay properties of the isomeric states in ^{95}Ag, ^{97}Ag and ^{97}Cd would help future shell-model investigations to make a proper choice of both the model space and the effective interaction to be used.

Acknowledgement

We want to thank Hubert Grawe for enlightening discussions as well as for a careful reading of the manuscript. The authors from Warsaw would like to kindly acknowledge the support and hospitality of GSI. This work was supported in part by the Polish Committee of Scientific Research under Grant KBN 2 P03B 039 013.

References

[1] R. Schneider, J. Friese, J. Reinhold, K. Zeitelhack, T. Faesterman, R. Gernhäuser, H. Gilg, F. Heine, J. Homolka, P. Kienle, H.J. Körner, H. Geissel, G. Münzenberg, and K. Sümmerer, Z. Phys. **A348** (1994) 221.

[2] M. Lewitowicz, R. Anne, G.Auger, D. Bazin, C. Borcea, V. Borrel, J.M. Corre, M. Huyse, Z. Janas, H. Keller, S. Lukyanov, A.C. Mueller, Yu. Penionzhkevich, M. Pfützner, F. Pougheon, K. Rykaczewski, M.G. Saint-Laurent, K. Schmidt, W.D. Schmidt-Ott, O. Sorlin, J. Szerypo, O. Tarasov, J. Wauters, and J. Żylicz, Phys. Lett. **B332** (1994) 20.

[3] M. Chartier, G. Auger, W. Mittig, A. Lepine-Szily, L. K. Fifield, , J.M. Casandjian, M. Chabert, J. Ferme, A. Gillibert, M. Lewitowicz, M. Mac Cormick, M.H. Moscatello, O.H. Odland, N.A. Orr, G. Politi, C. Spitaels, and A.C.C. Villari, Phys. Rev. Lett. **77** (1996) 2400.

[4] E. Roeckl, Nucl. Phys. **A583** (1995) 849.

[5] A. Guglielmetti, R. Bonetti, G. Poli, P.B. Price, A.J. Westphal, Z. Janas, H. Keller, R. Kirchner, O. Klepper, A. Piechaczek, E. Roeckl, K. Schmidt, A. Płochocki, J. Szerypo, and B. Blank, Phys. Rev. **C52** (1995) 740.

[6] E. Roeckl, Proc. of the Int. Nucl. Phys. Conf. (INPC'95), Beijing, 1995, eds. Sun Zuxun and Xu Jincheng (World Scientific, Singapore, 1996) 526.

[7] M. Hellström, Z. Hu, A. Weber, M. Henchek, M.J. Balbes, R.N. Boyd, D. Cano-Ott, R. Collatz, A. Guglielmetti, Z. Janas, M. Karny, R. Kirchner, J. Morford, D.J. Morrissey, G. Raimann, E. Roeckl, K. Schmidt, and J. Szerypo, Z. Phys. **A356** (1996) 229.

[8] K. Schmidt, Th.W. Elze, R. Grzywacz, Z. Janas, R.Kirchner, O. Klepper, A. Płochocki, E. Roeckl, K. Rykaczewski, L.D. Skouras, and J. Szerypo, Z. Phys. **A350** (1994) 99.

[9] I.S. Towner, Nucl.Phys. **A444** (1985) 402.

[10] I.P. Johnstone, Phys.Rev. **C44** (1991) 1476.

[11] L.D. Skouras and P. Manakos, J. Phys. **G19** (1993) 731.

[12] K. Rykaczewski, in *Nuclei Far From Stability / Atomic Masses and Fundamental Constants*, eds. R. Neugart and A. Wöhr, IOP Conf. Ser. No. 132, Section 5 (1993) 517.

[13] G. Walter, in *Nucl. Shapes and Nucl. Structure at Low Excitation Energies*, eds. M. Vergnes *et al.* (Edition Frontieres, 1994) 227.

[14] P.E. Haustein (ed.), 1986-1987 Atomic Mass Predictions, Atomic Data and Nucl. Data Tables **39** (1988) 185.

[15] G. Audi and A.H. Wapstra, Nucl. Phys. **A565** (1993) 1.

[16] K. Ogawa, Phys. Rev. **C28** (1983) 958.

[17] H. Grawe, R. Schubart, K.H. Maier, and D. Seweryniak, Physica Scripta **56** (1995) 71.

[18] R. Kirchner, O. Klepper, D. Marx, G.E. Rathke, and B. Sherill, Nucl. Instr. Meth. in Phys. Res. **A247** (1986) 265.

[19] R. Kirchner, Nucl. Instr. and Meth. in Phys. Res. **B70** (1992) 186.

[20] K. Schmidt, Ph. D. Thesis, Universtät Frankfurt am Main (1995), unpublished.

[21] E. Nolte and H. Hick, Z. Phys. **A305** (1982) 289.

[22] W. Kurcewicz, E.F. Zganjar, R. Kirchner, O. Klepper, E. Roeckl, P. Komninos, E. Nolte, D.Schardt, and P. Tidemand-Petersson, Z. Phys. **A308** (1982) 21.

[23] S.E. Arnell, D. Foltescu, H.A. Roth, O. Skeppstedt, J. Blomqvist, A. Nilsson, T. Kuroyanagi, S. Mitarai, and J. Nyberg, Phys. Rev. **C49** (1994) 51.

[24] W.F. Piel Jr, G. Scharff-Goldhaber, C.J. Lister, and B.J. Varely, Phys. Rev. **C28** (1983) 209.

[25] D. Alber, H.H. Berschat, H. Grawe, H. Haas, and P. Spellmeyer, Z. Phys. **A332** (1989) 129.

[26] B. Jonson and G. Nyman, in *Nuclear Decay Modes*, ed. D. N. Poenaru, (IOP, 1996) 102.

[27] N.B. Gove and M.J. Martin, Nuclear Data Tables **10** (1971) 205.

[28] M. Huyse, K. Cornelis, G. Dumont, G. Lhersonneau, J. Verplancke, and W.B. Walters, Z. Phys. **A288** (1978) 107.

[29] P. Fettweis, P. del Marmol, M. Degreef, P. Duhamel, and J. Vanhorenbeeck Z. Phys. **A305** (1982) 57.

[30] W.F. Piel Jr, D.B. Fossan, R. Ma, E.S. Paul, and N. Xu, Phys. Rev. **C41** (1990) 1223.

[31] D. Alber, H.H. Bertschat, H. Grawe, H. Haas, B. Spellmeyer, and X. Sun Z. Phys. **A355** (1990) 265.

[32] T. Elmroth, E. Hagberg, P.G. Hansen, J.C. Hardy, B. Jonson, H.L. Ravn, and P. Tidemand-Petersson, Nucl. Phys. **A304** (1978) 493.

[33] J. Sinatkas, L.D. Skouras, D. Strottman, and J.D. Vergados, J. Phys. **G18** (1992) 1377.

[34] J. Sinatkas, L.D. Skouras, D. Strottman, and J.D. Vergados, J. Phys. **G18** (1992) 1400.

[35] D.H. Gloeckner and F.J.D. Serduke, Nucl. Phys. **A220** (1974) 477.

[36] F.J.D. Serduke, R.D. Lawson, and D.H. Gloeckner, Nucl. Phys. **A256** (1976) 45.

[37] R. Gross and A. Frenkel, Nucl. Phys. **A267** (1976) 85.

[38] I.P. Johnstone and L.D. Skouras, Phys. Rev. **C55** (1997) 1227.

[39] A. Płochocki, K. Rykaczewski, T. Batsch, J. Szerypo, J. Żylicz, R. Barden, O. Klepper, E. Roeckl, D. Schardt, H. Gabelmann, P. Hill, H. Ravn, T. Thorsteinsen, I.S. Grant, H. Grawe, P. Manakos, L.D. Skouras, and the ISOLDE Collaboration, Z. Phys. **A342** (1992) 43.

[40] B.A. Brown and K. Rykaczewski, Phys. Rev. **C50** (1994) 2270.

[41] P.C. Divari, L.D. Skouras, and I.P. Johnstone, in preparation.

[42] I.P. Johnstone and L.D. Skouras, Phys. Rev. **C51** (1995) 2817

[43] P. Hornshøj, K. Wilsky, P.G. Hansen, and B. Jonson, Nucl. Phys. **A187** (1972) 609.

[44] M. Karny, J.M. Nitschke, L.F. Archambault, K. Burkard, D. Cano-Ott, M. Hellström, W. Hüller, R. Kirchner, S. Lewandowski, E. Roeckl, and A. Sulik, Nucl. Instr. and Meth. in Phys. Res. **B**, in press.

Figure Captions

Fig. 1. 1200-1400 keV section of the singles γ-ray spectrum measured for mass 95. The spectrum was obtained by using a cycle time of 8 s, and represents the sum of all time-subgroups. The strongest β-delayed γ-rays from the decay of ^{95}Ag and ^{95}Pd are marked. The other γ-rays, except for the unassigned 1219.3 keV line (see text), are from room background.

Fig. 2. ^{95}Ag decay scheme. Together with the experimental ^{95}Pd level energies, the predictions of low-lying positive-parity states from Model-1 are shown.

Fig. 3. Energy spectrum measured for β-delayed protons emitted in the decay of ^{96}Ag. The inset shows the experimental time characteristic of this activity along with the result of a least-squares fit yielding a half-life of (5.22 ± 0.15) s.

Fig. 4. ^{96}Ag decay scheme. The apparent β-intensities I per ^{96}Ag decay and the apparent *log ft* values represent estimates based on the experimental $\beta\gamma$ and βp data, and have unknown systematical uncertainties.

Fig. 5. ^{97}Ag decay scheme. The apparent β-intensities I per ^{97}Ag decay and the apparent *log ft* values represent estimates based on the experimental $\beta\gamma$ data, and have unknown systematical uncertainties.

Fig. 6. Energy spectrum measured for β-delayed protons emitted in the decay of ^{97}Cd (solid-line histogramm), together with the corresponding Model-1 prediction (dotted-line histogramm). The inset shows the experimental time characteristic of this activity along with the result of a least-squares fit yielding a half-life of (2.8 ± 0.6) s.

Fig. 7. Core polarization diagram used for correcting the bare GT operator in Model-1 and Model-2 calculations.

Fig. 8. Energy spectra of ^{95}Ag calculated by Ogawa [16] and by using Model-1. The number on the right of each level represents $2J^{\pi}$. Above 2 MeV only the lowest state for each J^{π} case is shown.

Fig. 9. B(GT) distribution for the decay of the $9/2^+$ ground-state of ^{95}Ag, calculated by using Model-1.

Fig. 10. Experimental B(GT) distribution for the decay of ^{96}Ag (lower panel) and B(GT) predictions deduced from Model-1 for the decay of the 8^+ and 2^+ states of ^{96}Pd. The predictions are shown as full and open bars, respectively.

Fig. 11. Energy spectra of ^{97}Ag calculated by using Model-1 and Model-2. The number on the right of each level represents $2J^{\pi}$. Above 2 MeV only the lowest state for each J^{π} case are shown.

Fig. 12. Experimental B(GT) distribution for the decay of ^{97}Ag (upper panel, histogram), including the observation limit (upper panel, solid line), and corresponding B(GT) predictions deduced from Model-1 (central panel) and Model-4 (lower panel), respectively.

Fig. 13. Yrast spectra of ^{97}Cd calculated by Ogawa [16] and by using Model-1 and Model-2. The number on the right of each level represents $2J^{\pi}$.

Table 1
Compilation of half-lives, measured in this work, and Q_{EC}, S_p, and (Q_{EC} - S_p) values, deduced from experiments or mass predictions, for $^{95-97}$Ag and ^{97}Cd. In addition, Q_{EC} values from shell-model calculations are given (see text).

Nucleus	Decay mode	$T_{1/2}$ (s)	Q_{EC} (MeV)	S_p (MeV)	Q_{EC} - S_p (MeV)	Q_{EC} (MeV) Shell model
^{95}Ag	βp	2.0±0.1	~10.6 [a]	4.51±0.60 [b]	~6.1	10.67
	$\beta\gamma$	1.74±0.13				
^{96}Ag	βp	5.22±0.15	11.60±0.53 [b]	5.12±0.21[c]	6.48±0.57	11.83
	$\beta\gamma$	4.50±0.06				
^{97}Ag	$\beta\gamma$	25.3±0.3	7.0±0.5 [b]	5.46±0.30[c]	1.5±0.6	6.76
^{97}Cd	βp	2.8±0.6	~9.3[a]	1.91±0.43 [b]	~7.4[c]	10.54

[a] Typical results obtained by mass predictions [14]
[b] Value and uncertainty at least partly estimated from systematic trends of experimental masses [15]
[c] Experimental data [15]

Table 2
Experimental parameters

Nucleus	Reaction	Beam Energy (MeV/u)	Target (mg/cm^2)	Detector Set-up	Cycle time (s)	T_{meas} (h)
^{95}Ag	^{58}Ni(^{40}Ca,p2n)^{95}Ag	4.2	3.0	$\Delta E - E$	24, 16, 8	23
^{95}Ag	^{58}Ni(^{40}Ca,p2n)^{95}Ag	4.0,4.5	3.0, 3.3	$\gamma - \gamma - X$	4.8	33
^{96}Ag	^{60}Ni(^{40}Ca,p3n)^{96}Ag	4.1	3.0	$\Delta E - E$	12	17
^{97}Ag	^{60}Ni(^{40}Ca,p2n)^{96}Ag	4.1	3.0	$\gamma - \gamma - X$	40, 12	17
^{97}Cd	^{60}Ni(^{40}Ca,3n)^{97}Cd	4.2	3.1	$\Delta E - E$	6	8.3

Table 3
Transition energies, relative intensities, half-lives and coincidence relations for the γ-lines attributed to the decay of the isotope ^{95}Ag. The intensities were normalized to the sum of all transitions from excited levels to the ground state of ^{95}Pd.

E_γ(keV)	Intensity(%)	$T_{1/2}$(s)	Coincident transitions
1261.2	43.5(3.5)	1.82 ± 0.23	K_αPd, 511.0, 538.6
1685.4	29.6(2.7)	1.73 ± 0.20	511.0
2025.1	21.8(2.4)	1.73 ± 0.29	511.0
538.6	9.0(1.4)	-	511.0,1261.2
1799.8	5.1(2.4)	-	-
K_αPd	-	1.60 ± 0.36	1261.2

Table 4
Transition energies, relative intensities, half-lives and coincidence relations for γ-lines assigned to the decay of ^{96}Ag.

E_γ(keV)	Intensity(%)	$T_{1/2}$(s)	Coincident transitions
106.6	39(4)	4.37 ± 0.09	325.3, 684.0, 1415.5, K_αPd, K_βPd
325.3	91(9)	4.64 ± 0.13	106.6, 511.0, 684.0, 1415.5, K_αPd, K_βPd
684.0	93(9)	4.13 ± 0.19	106.6, 325.3, 511.0, K_αPd, K_βPd
1415.5	100(9)	4.91 ± 0.48	106.6, 325.3, 511.0, 684.0, K_αPd
K_αPd	-	4.65 ± 0.10	106.6, 325.3, 684.0, 1415.5

Table 5
Transition energies, absolute intensities per decay, half-lives and coincidence relations for γ-lines associated with the decay of ^{97}Ag.

E_γ(keV)	Intensity(%)	$T_{1/2}$(s)	Coincident transitions
351.9	2.0(0.2)	-	511, 586.2, 1294.5, 1594.8
445.9	2.3(0.3)	-	511, 845.5, 1151.3, 1294.5
495.3	1.9(0.2)	-	511, 586.2, 1294.5
586.2	8.1(0.8)	27.1 ± 1.7	351.9, 493.5, 511, 1006.7, 1294.5
608.7	3.3(0.3)	-	511, 685.8, 845.5, 1151.3
637.7	1.3(0.2)	-	511, 1537.4
685.8	64.5(6.6)	25.4 ± 0.4	511, 608.7, 1256.3, 1447.9, 1489.3, 1562.1
			1658.0, 2664.6, 3051.4, 3294.0
845.5	4.6(0.5)	-	445.9,511, 608.7, 1151.3, 1294.5
1006.7	0.9(0.1)	-	511, 586.2, 1294.5
1101.0	2.4(0.4)	-	511, 1294.5
1151.3	2.6(0.4)	-	445.9, 511, 845.5, 1294.5
1210.5	2.2(0.3)	-	511, 1294.5
1256.3	10.4(1.1)	26.3 ± 1.5	511, 685.8
1294.5	26.9(2.8)	24.7 ± 0.7	351.9, 445.9, 493.5, 511, 586.2, 845.5
			1151.3, 1210.5, 1101.0
1447.9	2.4(0.3)	-	511, 685.8
1489.3	7.7(0.8)	-	511, 685.8, 1562.1
1537.9	6.2(0.7)	25.9 ± 2.1	511, 637.7
1562.1	2.1(0.2)	-	511, 685.8, 1489.3
1594.8	1.5(0.2)	-	351.9, 511
1658.0	2.0(0.2)	-	511, 685.8
1880.7	0.7(0.1)	-	-
2374.2	1.6(0.2)	-	511
2664.6	2.1(0.3)	-	511, 685.8
3051.4	4.6(0.5)	25.3 ± 2.6	511, 685.8
3294.0	2.9(0.3)	24.1 ± 2.8	511, 685.8
K_αPd	-	-	511, 685.8

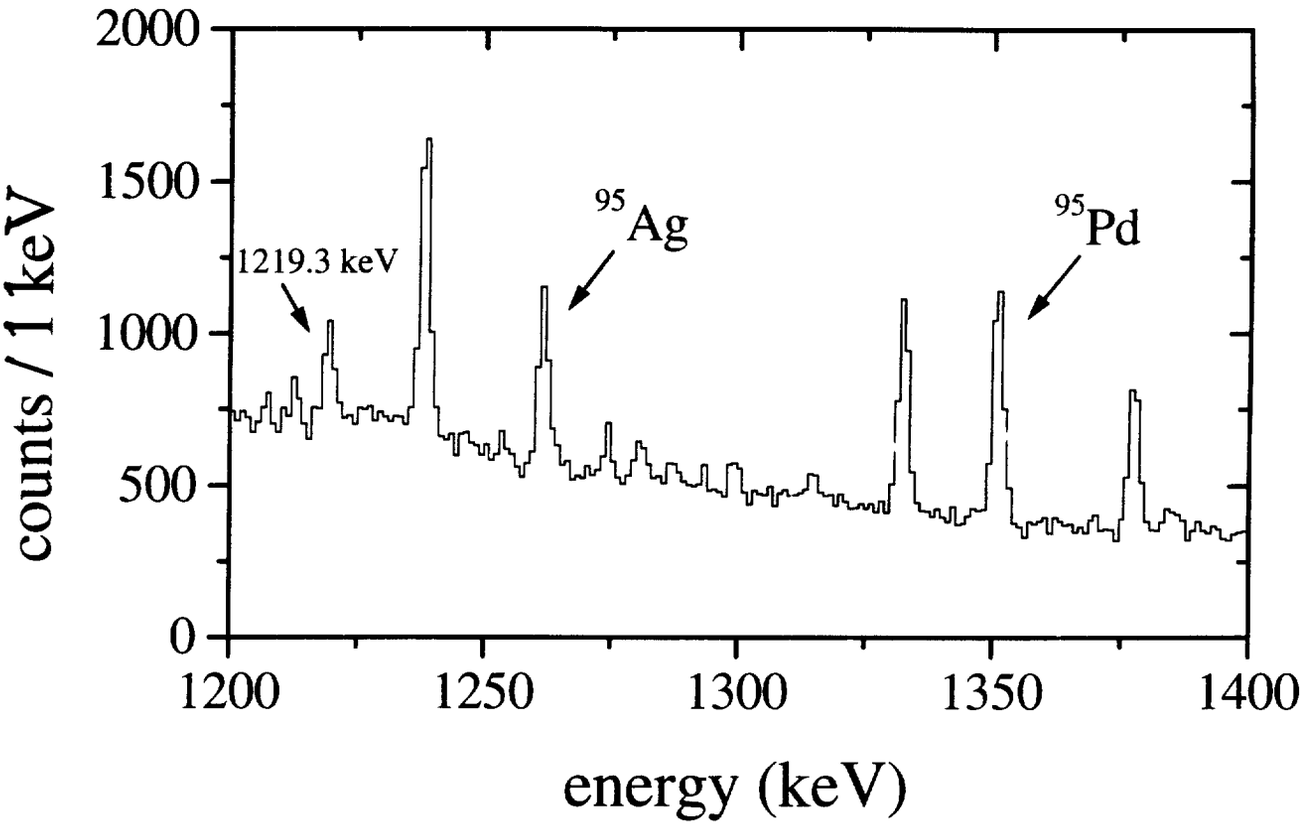
2000
1500
1000
500
0
counts / 1 keV
1219.3 keV
95Ag
95Pd
1200
1250
1300
1350
1400
energy (keV)

Fig. 1

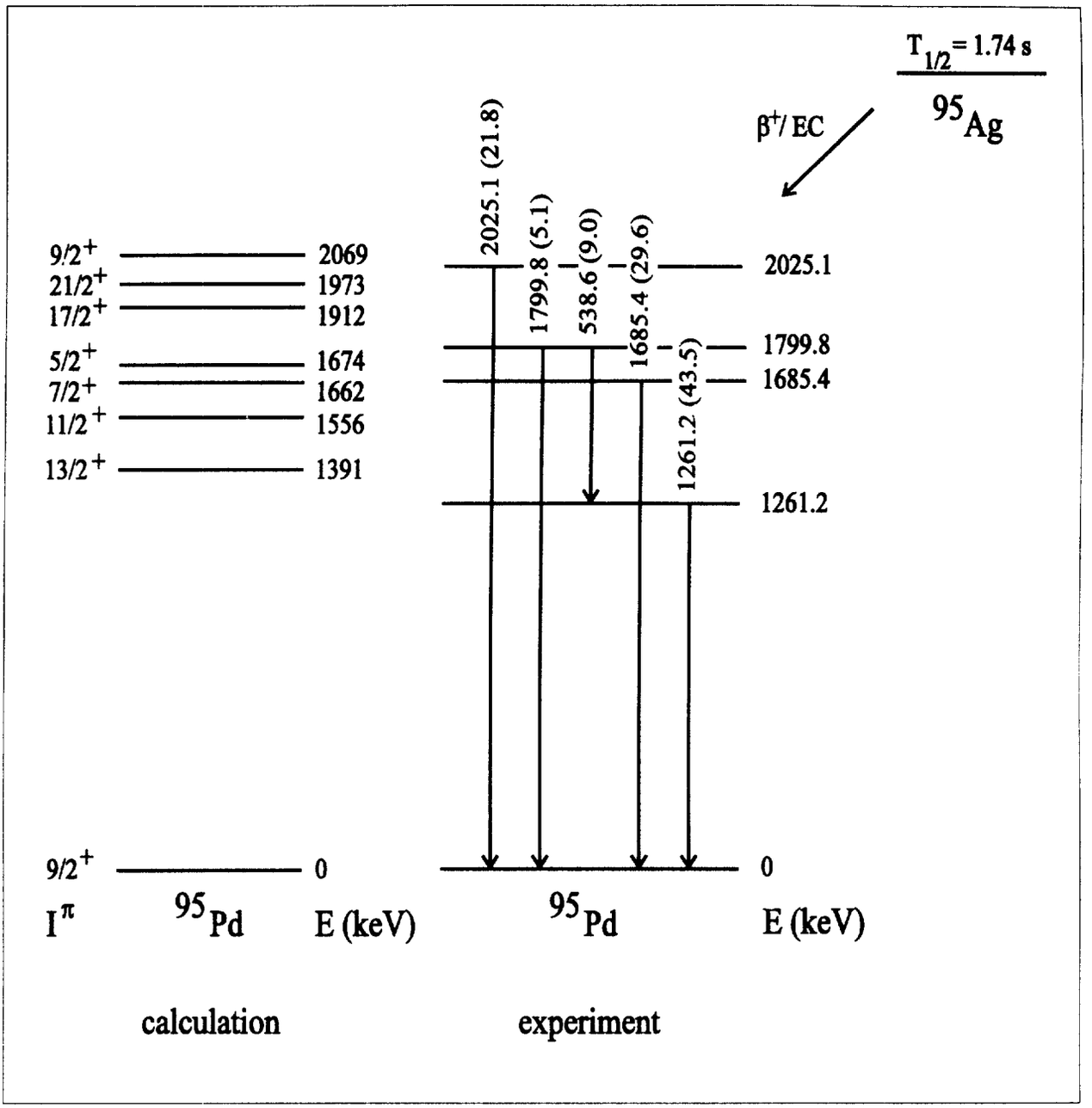
$T_{1/2}$ = 1.74 s
^{95}Ag
β+/ EC
2025.1 (21.8)
1799.8 (5.1)
538.6 (9.0)
1685.4 (29.6)
1261.2 (43.5)
9/2+ 2069
21/2+ 1973
17/2+ 1912
5/2+ 1674
7/2+ 1662
11/2+ 1556
13/2+ 1391
9/2+ 0
2025.1
1799.8
1685.4
1261.2
0
Iπ
^{95}Pd
E (keV)
^{95}Pd
E (keV)
calculation
experiment

Fig. 2

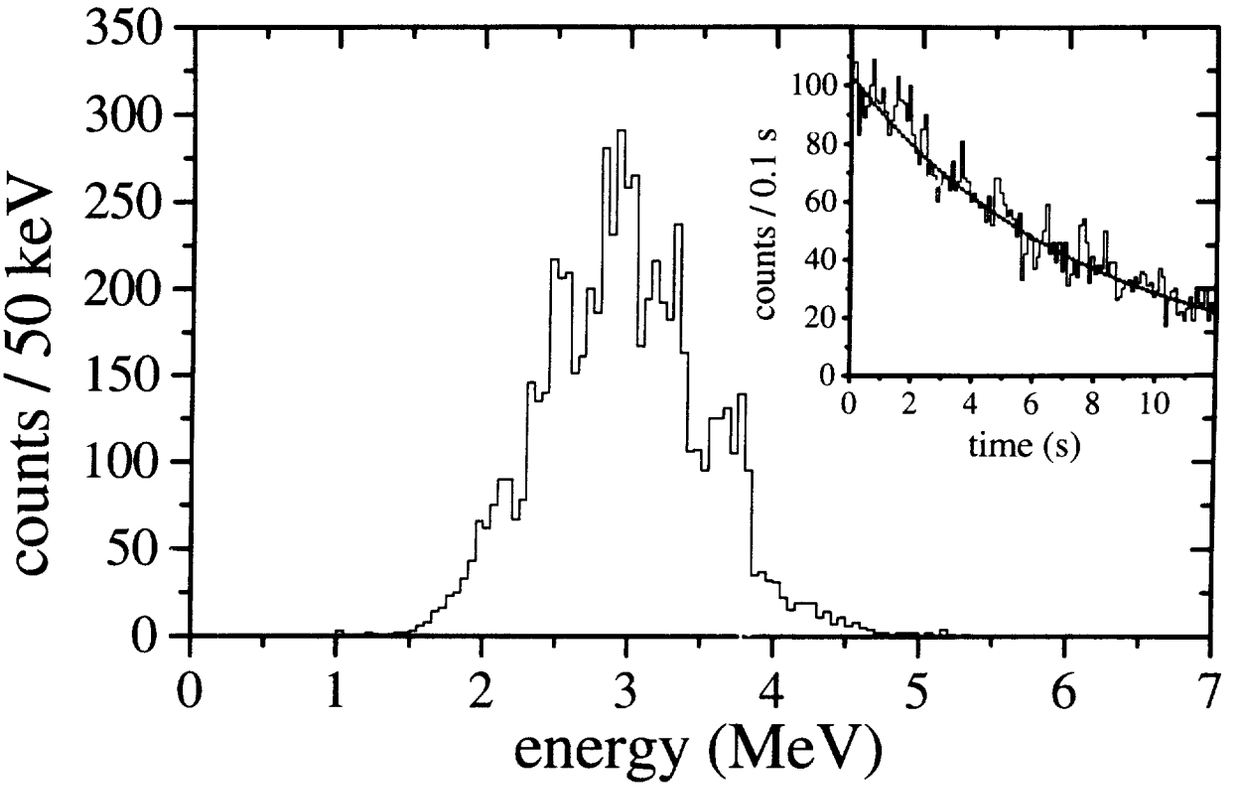

Fig. 3

Fig. 4

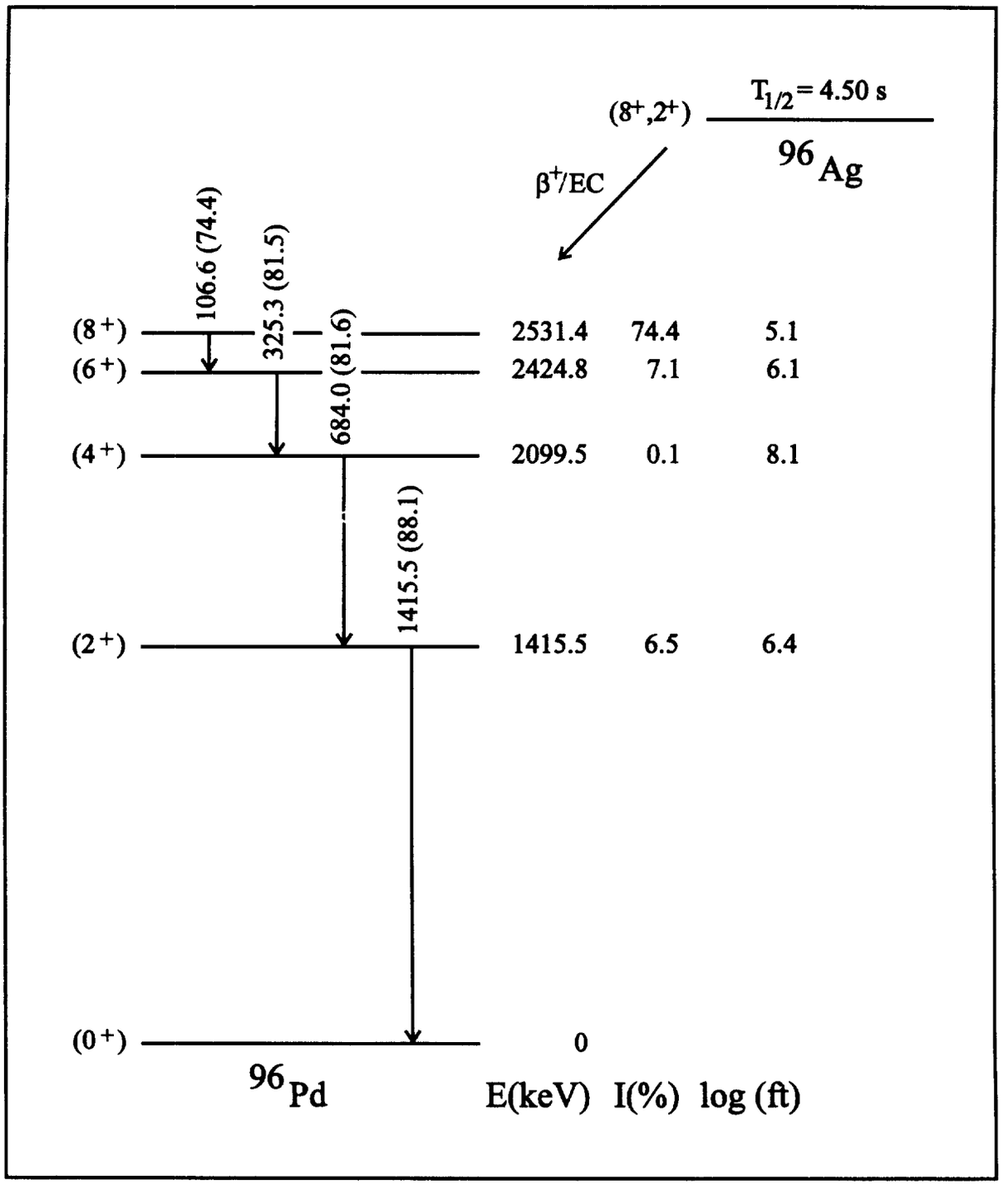
(8+,2+)
T1/2 = 4.50 s
96 Ag
β+/EC
106.6 (74.4)
325.3 (81.5)
684.0 (81.6)
1415.5 (88.1)
(8+)
(6+)
(4+)
(2+)
(0+)
2531.4 74.4 5.1
2424.8 7.1 6.1
2099.5 0.1 8.1
1415.5 6.5 6.4
0
96 Pd
E(keV) I(%) log (ft)

Fig. 5

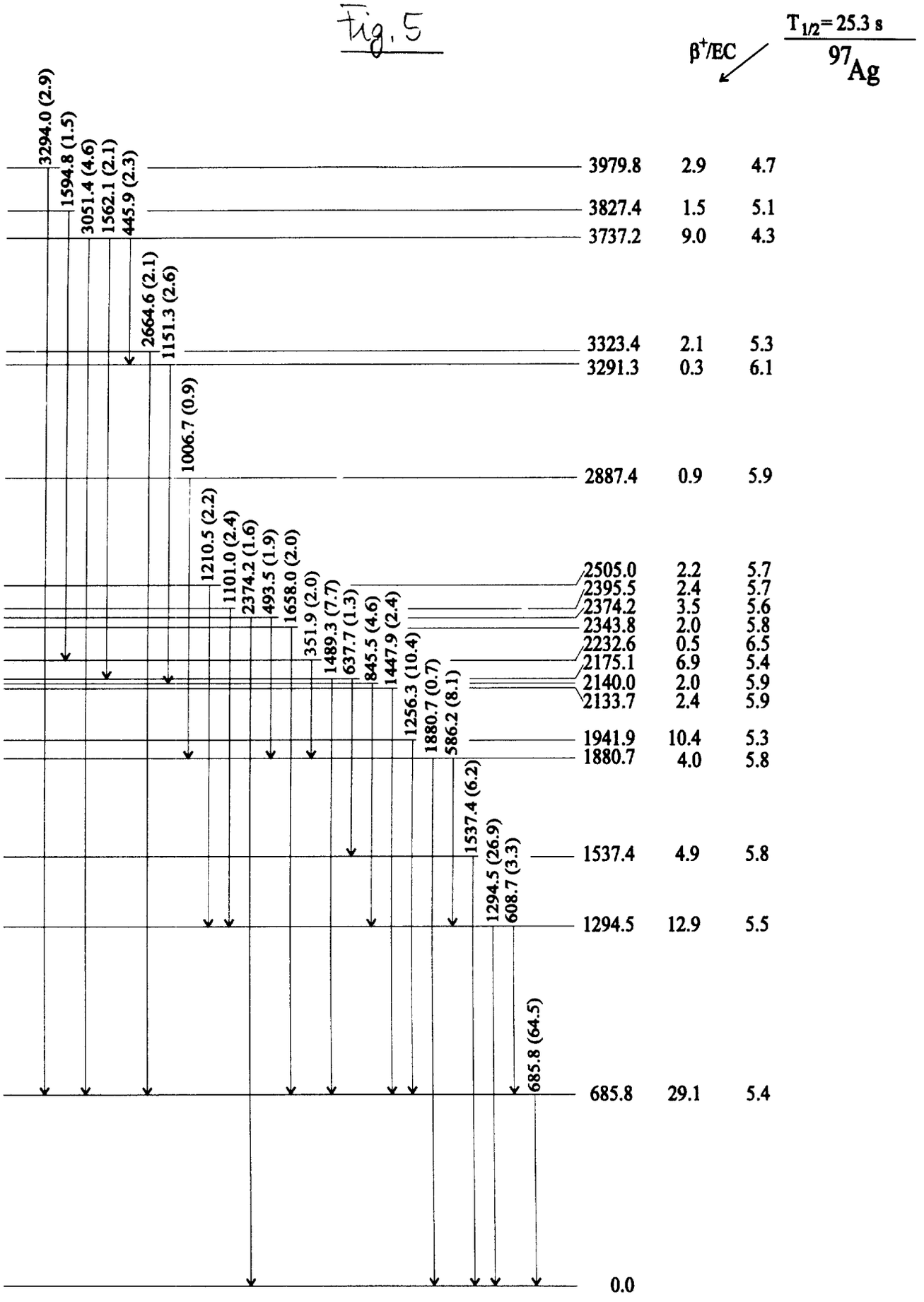
$T_{1/2}$= 25.3 s
β^+/EC
^{97}Ag
3294.0 (2.9)
1594.8 (1.5)
3051.4 (4.6)
1562.1 (2.1)
445.9 (2.3)
2664.6 (2.1)
1151.3 (2.6)
1006.7 (0.9)
1210.5 (2.2)
1101.0 (2.4)
2374.2 (1.6)
493.5 (1.9)
1658.0 (2.0)
351.9 (2.0)
1489.3 (7.7)
637.7 (1.3)
845.5 (4.6)
1447.9 (2.4)
1256.3 (10.4)
1880.7 (0.7)
586.2 (8.1)
1537.4 (6.2)
1294.5 (26.9)
608.7 (3.3)
685.8 (64.5)
3979.8 2.9 4.7
3827.4 1.5 5.1
3737.2 9.0 4.3
3323.4 2.1 5.3
3291.3 0.3 6.1
2887.4 0.9 5.9
2505.0 2.2 5.7
2395.5 2.4 5.7
2374.2 3.5 5.6
2343.8 2.0 5.8
2232.6 0.5 6.5
2175.1 6.9 5.4
2140.0 2.0 5.9
2133.7 2.4 5.9
1941.9 10.4 5.3
1880.7 4.0 5.8
1537.4 4.9 5.8
1294.5 12.9 5.5
685.8 29.1 5.4
0.0
^{97}Pd
E (keV) I(%) log (ft)

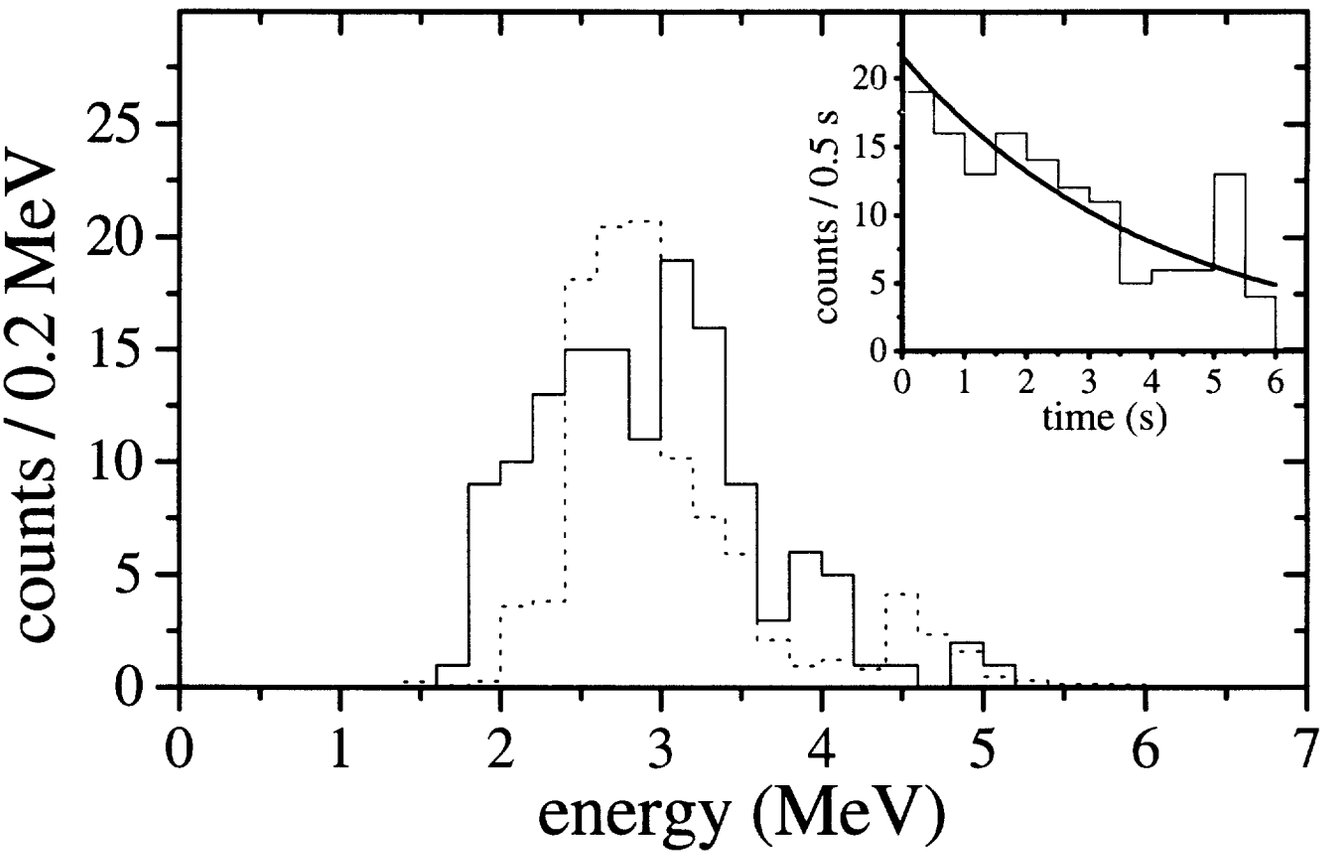

Fig. 6

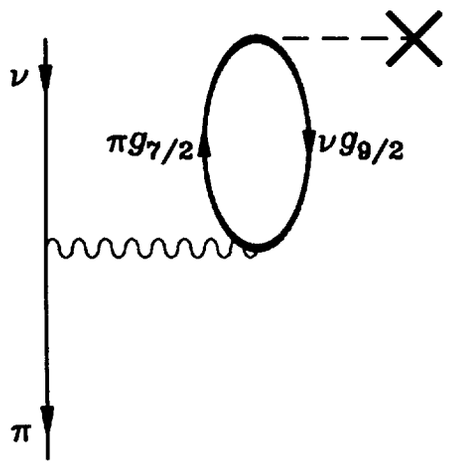

Model–1

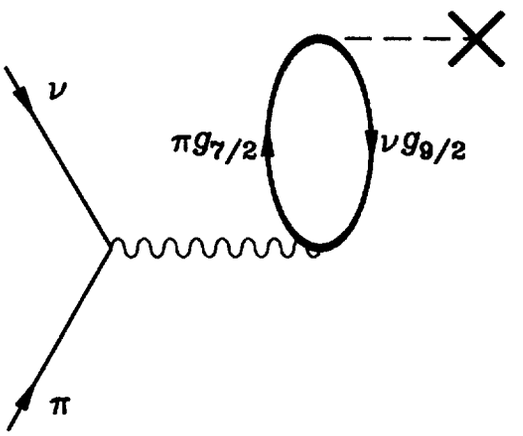

Model–2

Fig. 7

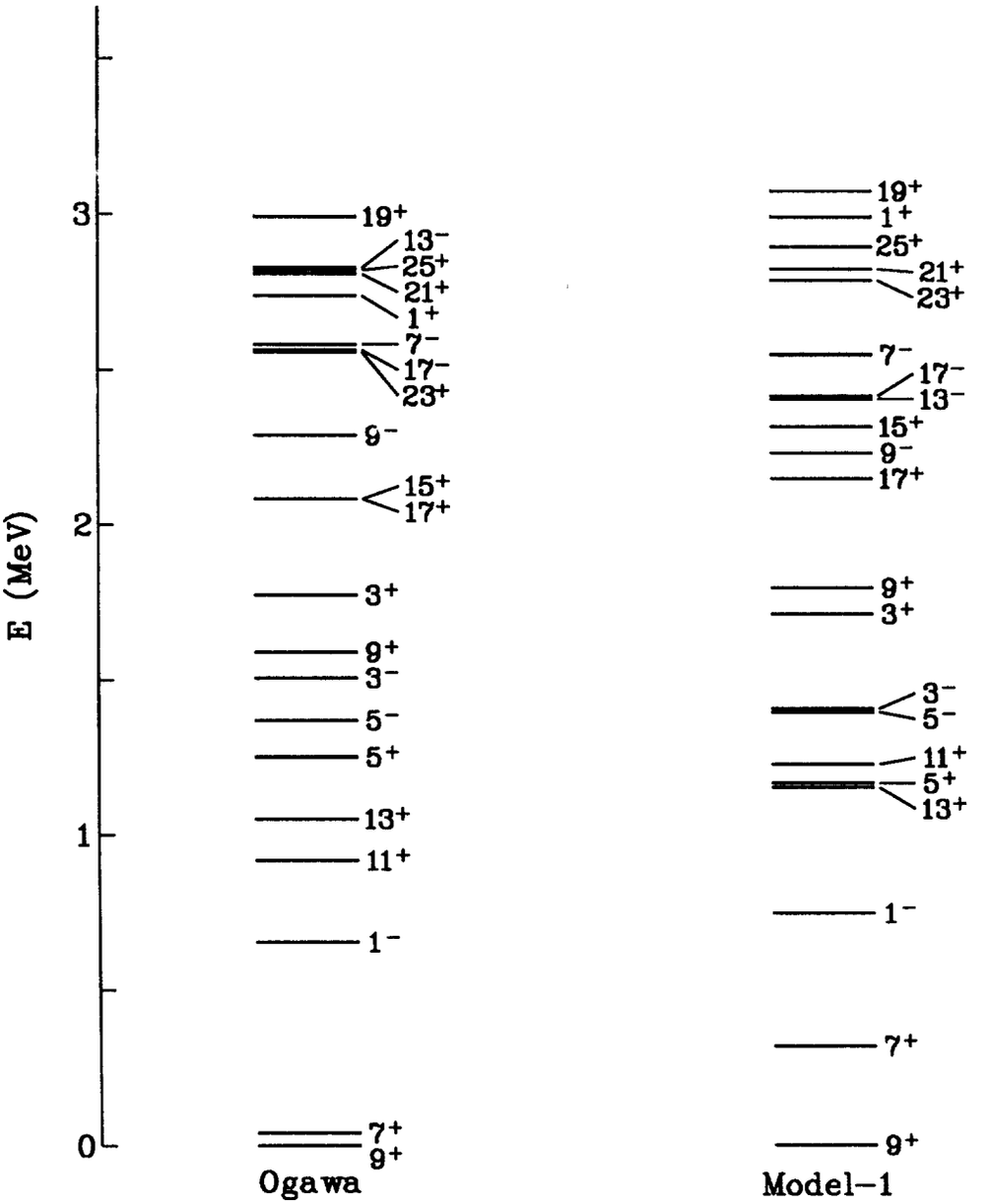
E (MeV)
3
2
1
0
19+
13−
25+
21+
1+
7−
17−
23+
9−
15+
17+
3+
9+
3−
5−
5+
13+
11+
1−
7+
9+
Ogawa
19+
1+
25+
21+
23+
7−
17−
13−
15+
9−
17+
9+
3+
3−
5−
11+
5+
13+
1−
7+
9+
Model−1

^{95}Ag

Fig. 8

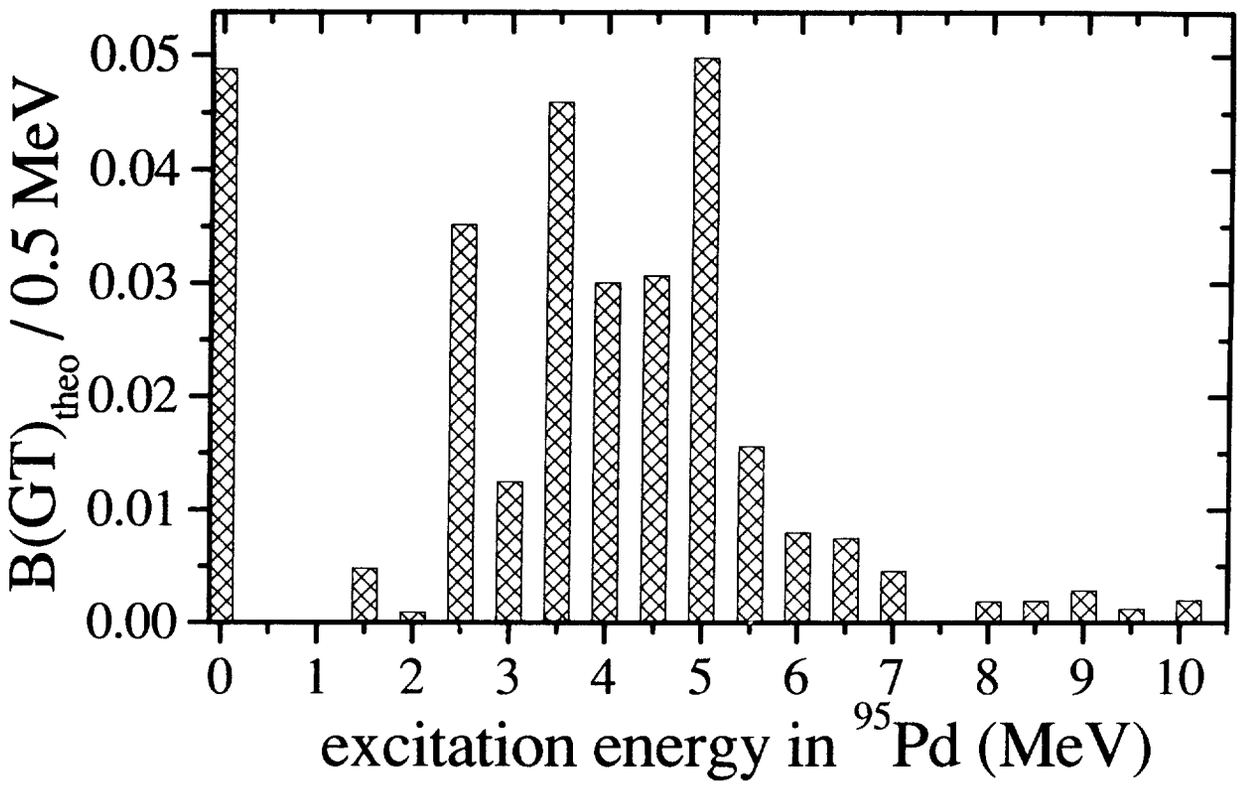
0.05
0.04
0.03
0.02
0.01
0.00
B(GT)theo / 0.5 MeV
0
1
2
3
4
5
6
7
8
9
10
excitation energy in 95Pd (MeV)

Fig. 9

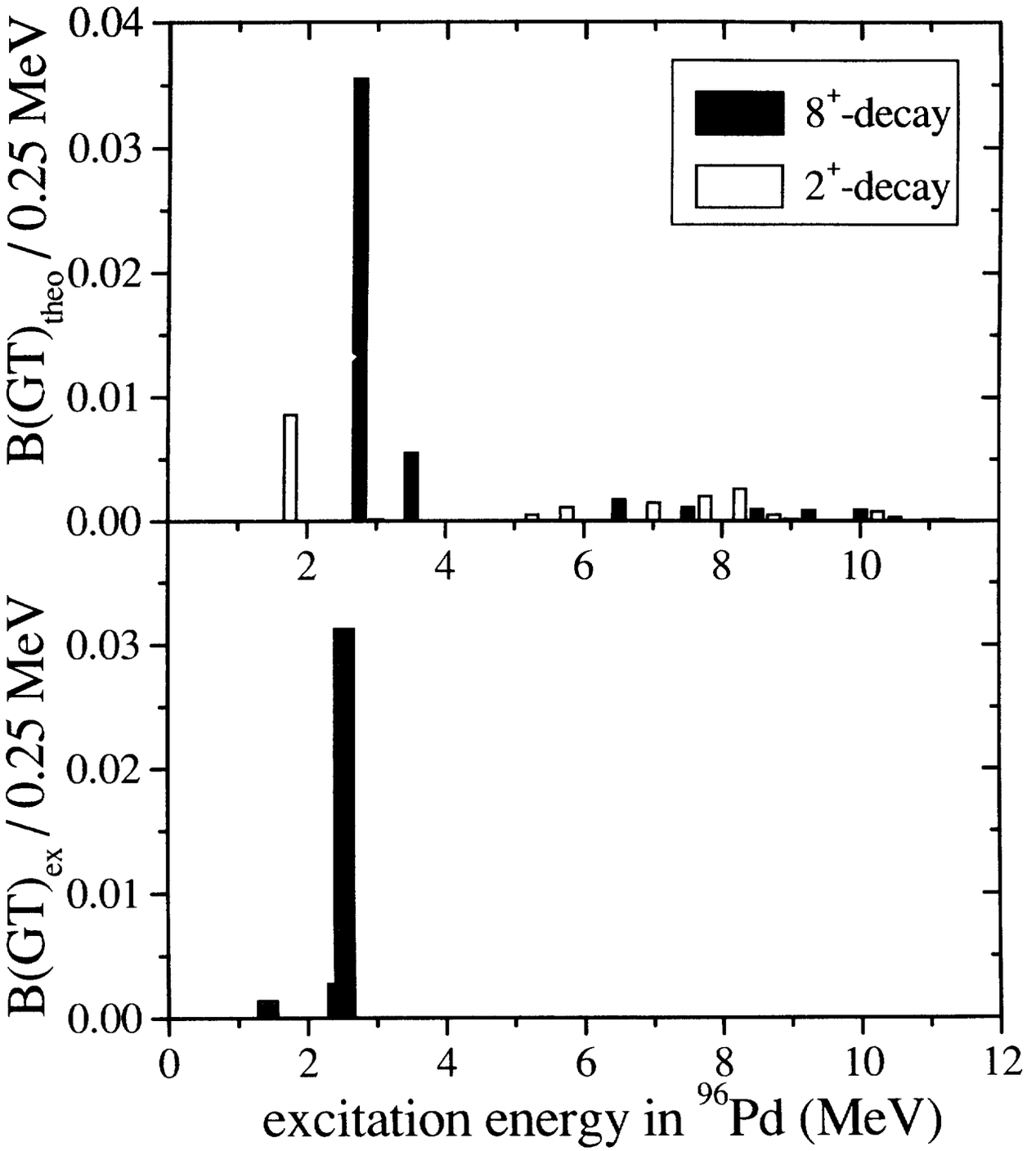
0.04
0.03
0.02
0.01
0.00
B(GT)theo / 0.25 MeV
8+-decay
2+-decay
2
4
6
8
10
0.03
0.02
0.01
0.00
B(GT)ex / 0.25 MeV
0
2
4
6
8
10
12
excitation energy in 96Pd (MeV)

Fig. 10

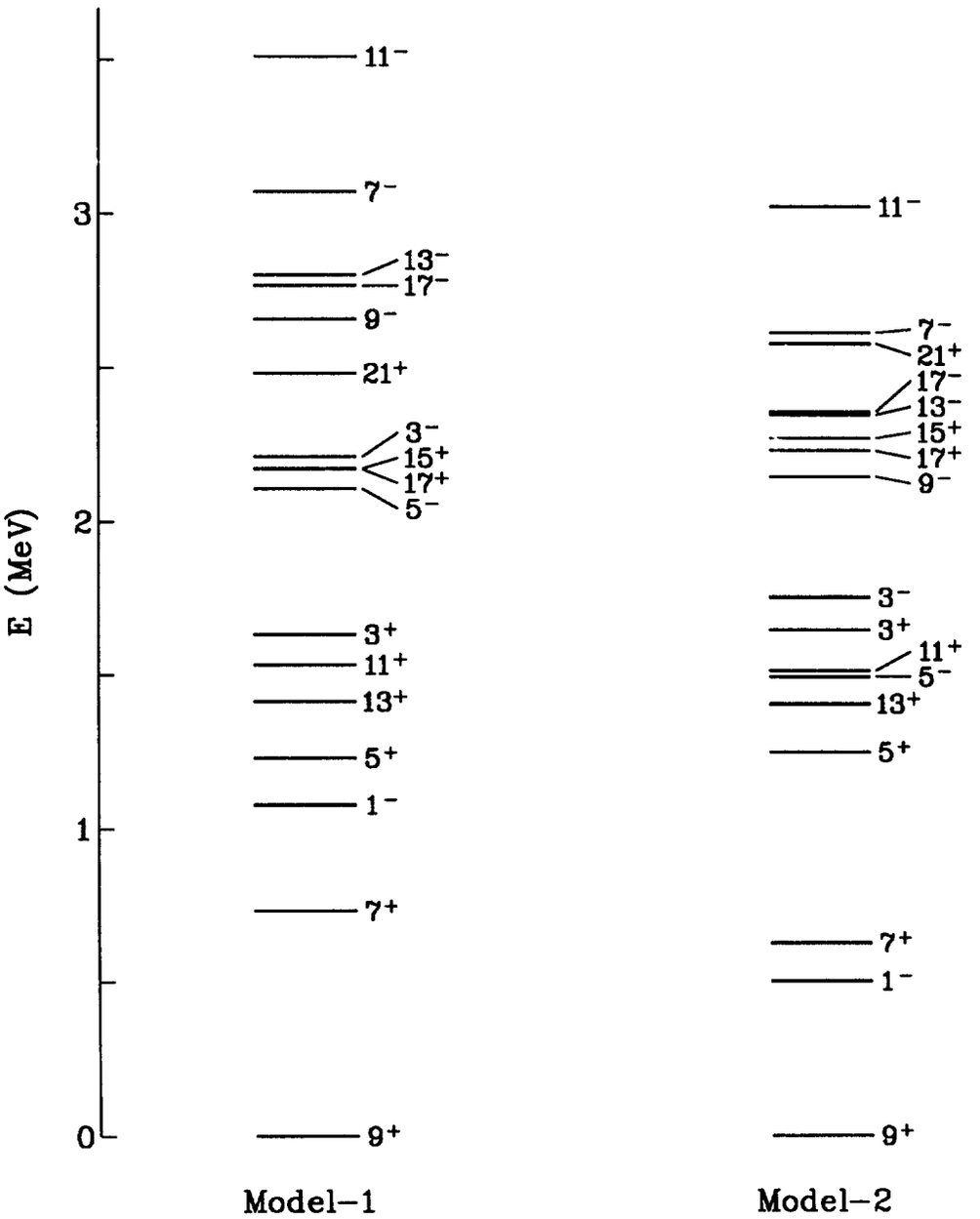
E (MeV)
0
1
2
3
11⁻
7⁻
13⁻
17⁻
9⁻
21⁺
3⁻
15⁺
17⁺
5⁻
3⁺
11⁺
13⁺
5⁺
1⁻
7⁺
9⁺
Model–1
11⁻
7⁻
21⁺
17⁻
13⁻
15⁺
17⁺
9⁻
3⁻
3⁺
11⁺
5⁻
13⁺
5⁺
7⁺
1⁻
9⁺
Model–2

^{97}Ag

Fig. 11

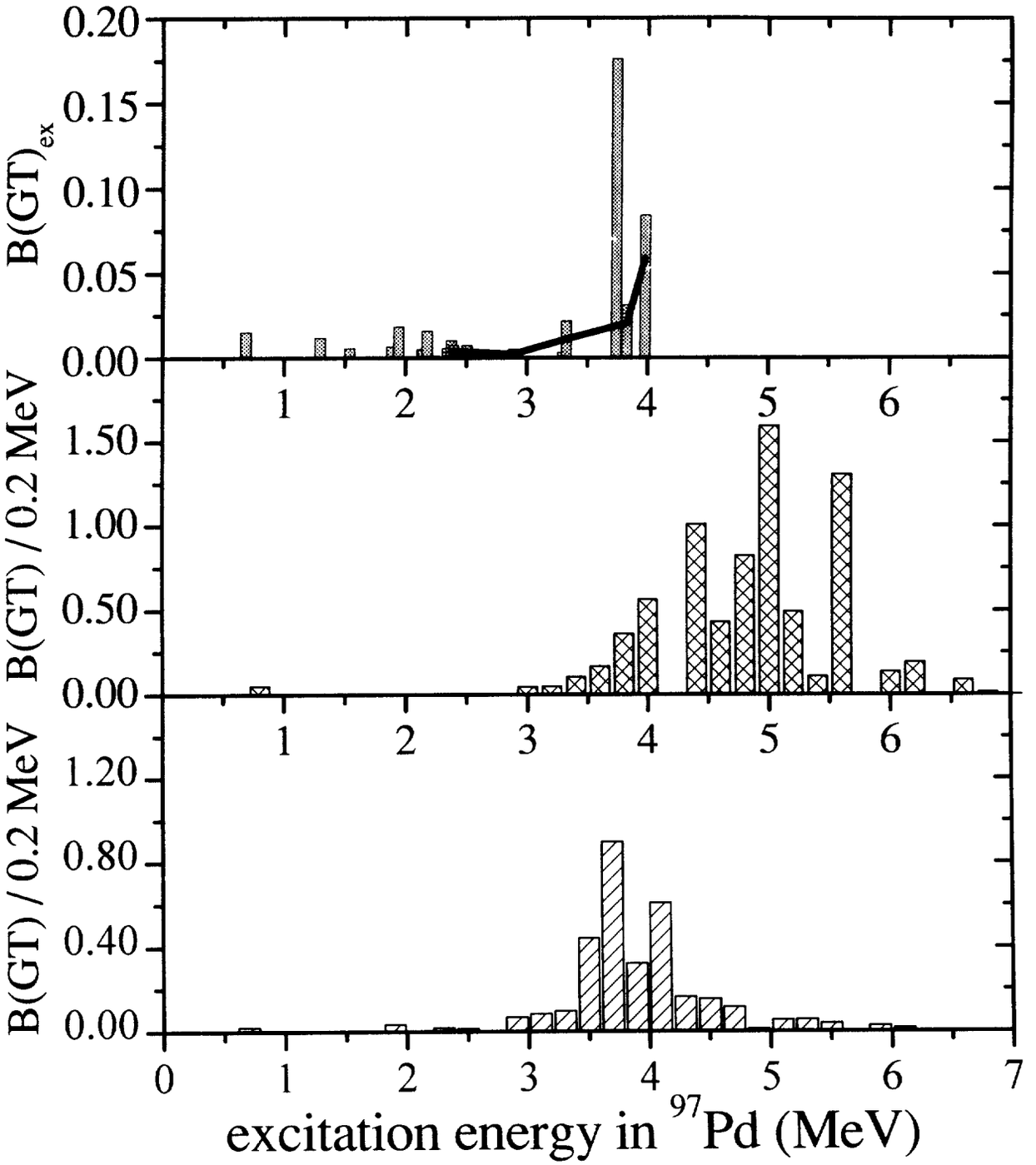
B(GT)_ex
0.20
0.15
0.10
0.05
0.00
1
2
3
4
5
6
B(GT) / 0.2 MeV
1.50
1.00
0.50
0.00
B(GT) / 0.2 MeV
1.20
0.80
0.40
0.00
0
1
2
3
4
5
6
7
excitation energy in 97Pd (MeV)

Fig. 12

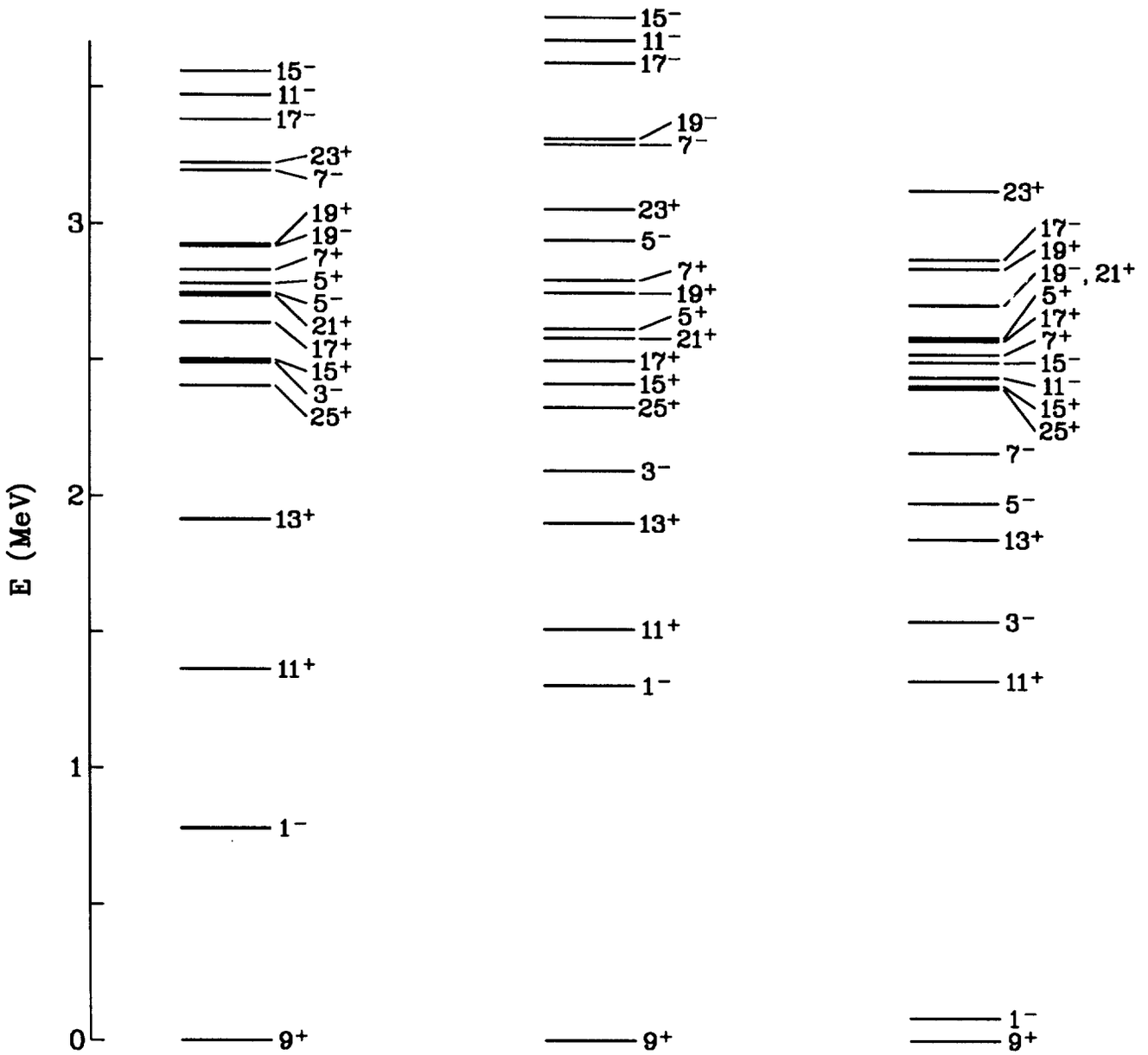
E (MeV)
0
1
2
3
15⁻
11⁻
17⁻
23⁺
7⁻
19⁺
19⁻
7⁺
5⁺
5⁻
21⁺
17⁺
15⁺
3⁻
25⁺
13⁺
11⁺
1⁻
9⁺
Ogawa
15⁻
11⁻
17⁻
19⁻
7⁻
23⁺
5⁻
7⁺
19⁺
5⁺
21⁺
17⁺
15⁺
25⁺
3⁻
13⁺
11⁺
1⁻
9⁺
Model-1
23⁺
17⁻
19⁺
19⁻, 21⁺
5⁺
17⁺
7⁺
15⁻
11⁻
15⁺
25⁺
7⁻
5⁻
13⁺
3⁻
11⁺
1⁻
9⁺
Model-2

^{97}Cd

Fig. 13